An Investigation of Unburned Hydrocarbon Emissions in Wall Guided, Low Temperature Diesel Combustion

J. Kashdan, S. Mendez, G. Bruneaux

Oil & Gas Science and Technology – Rev. IFP, Vol. 63 (2008), No. 4, pp. 433-459

DOI: 10.2516/ogst:2008018

Dossier

Diesel Engines and Fuels: a Wide Range of Evolutions to Come
Motorisation et carburants Diesel : un large spectre d'évolutions à venir

An Investigation of Unburned Hydrocarbon Emissions in Wall Guided, Low Temperature Diesel Combustion

J. Kashdan, S. Mendez and G. Bruneaux

Institut français du pétrole, IFP, Division Techniques d'Applications Énergétiques, 1-4 avenue de Bois-Préau, 92852 Rueil-Malmaison Cedex - France
e-mail: julian.kashdan@ifp.fr - sylvain.mendez@ifp.fr - gilles.bruneaux@ifp.fr

Résumé — Une investigation des émissions d'hydrocarbures imbrûlés en combustion Diesel à basse température avec guidage paroi — Les mécanismes de formation des hydrocarbures imbrûlés (HC) dans les systèmes de combustion à bas niveaux de NOx ont été investigués sur moteurs monocylindre opaque et optique fonctionnant à faible charge (2 et 4 bar de PMI). Sur moteur opaque, les paramètres tels que l'avance d'injection (AVI), la température plénum et la richesse globale ont été variés afin d'analyser le rôle du phénomène de quenching de masse sur la formation d'émissions de HC. La technique d'imagerie par fluorescence induite par laser (LIF) des HC imbrûlés à l'intérieur de la chambre a été appliquée sur le moteur optique. En outre, des essais ont été réalisés sur moteur opaque afin d'évaluer la contribution du volume mort du premier cordon sur les émissions de HC. Enfin, le rôle des films liquides et leur impact sur les émissions de HC ont été étudiés sur les deux types de moteurs. Sur moteur opaque l'investigation a consisté à comparer les résultats obtenus avec deux carburants dont les volatilités étaient différentes. En parallèle, la technique de LIF traceur a été appliquée sur moteur optique pour visualiser les films liquides.

Les résultats obtenus sur les moteurs opaque et optique ont mis en évidence que le quenching de masse est une source majeure d'émission de HC dans le cas d'une géométrie de combustion avec guidage paroi. Le quenching de masse est le résultat de l'oxydation partielle du carburant dans les zones où la richesse locale est soit trop pauvre, soit trop riche et/ou la température locale n'est pas suffisamment élevée. Les données expérimentales obtenues sur les deux moteurs ont également révélé la présence de films liquides, surtout pour des stratégies d'injections précoces. En outre, les films liquides restent présents en fin de combustion, contribuant aux émissions de HC. Les images de LIF des films liquides semblent montrer que les films se détachent de la surface du piston pendant la phase de détente par un phénomène de « flash boiling ». Ces résultats semblent donc confirmer que le carburant non-brûlé issu des films liquides contribue directement aux émissions de HC.

Abstract — An Investigation of Unburned Hydrocarbon Emissions in Wall Guided, Low Temperature Diesel Combustion — *The formation mechanisms of unburned hydrocarbons (HC) in low NOx, homogeneous type Diesel combustion have been investigated in both standard and optical access single cylinder engines operating under low load (2 and 4 bar IMEP) conditions. In the standard (i.e. non-optical) engine, parameters such as injection timing, intake temperature and global equivalence ratio were varied in order to analyse the role of bulk quenching on HC emissions formation. Laser-Induced*

Fluorescence (LIF) imaging of in-cylinder unburned HC within the bulk gases was performed on the optical-access engine. Furthermore, studies were performed in order to ascertain whether the piston top-land crevice volume contributes significantly to engine-out HC emissions. Finally, the role of piston-top fuel films and their impact on HC emissions was studied. This was investigated on the all-metal engine using two fuels of different volatilities. Parallel studies were also performed on the optical-access engine via in-cylinder tracer Laser-Induced Fluorescence (LIF) imaging.

Results obtained in the standard and optical access engines revealed that bulk quenching represents one of the most significant sources of unburned HC for the wall guided combustion chamber geometry. Bulk quenching occurs as a result of incomplete fuel oxidation reactions in regions where the local equivalence ratio is either too fuel-lean or too fuel-rich or alternatively in excessively low temperature zones within the combustion chamber. Experimental data obtained from both the standard and optical access engines also revealed that liquid film formation occurs, and is particularly prevalent for early Start Of Injection (SOI) strategies. Furthermore, liquid films remain present at the end of combustion and are believed to represent a significant source of engine-out HC emissions. In-cylinder imaging of liquid films suggest that the film eventually detaches from the piston surface later during the expansion stroke, resembling a flash boiling phenomenon. The results appear to confirm that unburned fuel arising from piston-top fuel films contribute directly to the engine-out HC emissions.

DEFINITIONS

CAD	Crank Angle Degree
CI	Compression Ignition
CO	Carbon Monoxide
DI	Direct Injection
EGR	Exhaust Gas Recirculation
EVO	Exhaust Valve Opening
FWHM	Full Width Half Maximum
HC	Hydrocarbons
HCCI	Homogeneous Charge Compression Ignition
IMEP	Indicated Mean Effective Pressure
LIF	Laser Induced Fluorescence
LTC	Low Temperature Combustion
NADI	Narrow Angle Direct-Injection
NOx	Oxides of Nitrogen
PAH	Poly-aromatic Hydrocarbons
PFI	Port Fuel Injection
RoHR	Rate of Heat Release
ROI	Region of Interest
RPM	Revolutions per Minute
SI	Spark Ignition
SOI	Start of Injection
TDC	Top Dead Centre
$T_{coolant}$	Coolant Temperature
T_{int}	Intake Temperature

INTRODUCTION

There is significant interest in homogeneous charge compression ignition (HCCI) or low temperature Diesel combustion (LTC) systems which enable considerable reductions of engine-out NOx and particulate emissions. This is primarily achieved by the production of a relatively homogeneous in-cylinder mixture distribution using either a fully pre-mixed fueling strategy or early direct injection strategies. In the former case, a homogeneous in-cylinder charge is often achieved by injecting fuel well upstream of the intake port. In general, this approach relies on a significant amount of charge pre-heating to fully vaporise the fuel air mixture. Alternatively, direct, in-cylinder injection of the fuel is another approach in which early start of injection (SOI) timings are adopted. In this case, large amounts of cooled Exhaust Gas Recirculation (EGR) are typically required in order to limit the heat release or pressure-rise rate. The lower combustion temperatures inhibit NOx production. Typically, the peak combustion temperatures that are attained in low NOx combustion systems are in the range of 1400 to 1800 K which is significantly lower compared to conventional Diesel engine combustion systems. In this latter case peak combustion temperatures often exceed 2400 K.

Despite the benefits offered by HCCI or low-temperature combustion systems, high levels of unburned HC and carbon monoxide (CO) emissions are observed particularly at low or part load operating conditions. The reduction of HC emissions "in-cylinder" is particularly important since the post oxidation of these species is made even more difficult due to the low exhaust gas temperatures encountered in HCCI or LTC combustion. The issue of elevated HC (and CO) emissions in HCCI or low-temperature Diesel combustion systems is widely recognised however, few experimental studies have been performed which offer an insight into the underlying mechanisms of HC emissions formation. The importance of piston top-land geometry was studied via experiments and modeling for a flat, "pancake" piston geometry [1, 2]. In this study, fuel was pre-mixed and pre-heated with air to ensure the formation of a homogeneous charge. It was shown that an

increase in the piston top-land crevice volume resulted in a significant increase in the HC emissions due to fuel trapping within this volume, a result which is well known for port fuel injected spark ignition engines [3]. Another experimental study was performed on a variable compression ratio HCCI engine fueled with n-butane [4] in which measurements of the exhaust gas species were made by Fourier transform infra-red (FT-IR) spectrometry. The results presented in Reference [4] indicated that unburned fuel trapped within combustion chamber crevice volumes might contribute to engine-out HC emissions. Furthermore, under low load engine operating conditions, intermediate species such as methane (CH_4), the alkenes ethane (C_2H_4) and propylene (C_3H_6) and aldehydes, formaldehyde (HCHO) and acetaldehyde (CH_3CHO) were detected. The concentration of these species was found to decrease with an increase in equivalence ratio (engine load) whilst the concentration of n-butane measured within the exhaust gases remained approximately constant. The authors suggested that these results indicated partial oxidation (*i.e.* incomplete combustion) of the fuel was occurring in the bulk gases at low load.

A recent, detailed experimental study on the combustion and in particular the CO emissions for a low temperature Diesel combustion system is reported in References [5, 6]. This investigation focused on the effects of various parameters such as charge dilution, swirl ratio and injection timing and revealed the significant role of in-cylinder mixing processes which impact CO emissions formation. In particular, a reduction in CO emissions with increased pre-combustion mixing was observed. It was proposed that the increase in pre-mixing was a result of an increased ignition delay due either to early SOI timings or by increasing the mixing rates using high swirl ratios. The results suggested that CO emissions are preferentially formed in locally fuel-rich zones (*i.e.* under-mixed fuel).

Experiments performed within the present study focus on the origin of HC emissions within a wall-guided, low-NOx combustion system in which a narrow angle multi-hole nozzle is utilised with an optimised piston bowl geometry. The so-called narrow angle direct injection (NADI™) approach developed at IFP enables dual mode Diesel combustion. Under low and part load engine operating conditions, premixed, low temperature/low-NOx combustion can be achieved. For higher load operating conditions, the NADI™ concept can be operated in conventional Diesel (diffusion-limited combustion) mode. Further details on the NADI™ concept have previously been reported in [7, 8].

POTENTIAL SOURCES OF HC EMISSIONS

In general, there are several sources of engine-out HC emissions which are briefly summarised. A more detailed description is provided in [3]. Trapping of fuel in combustion chamber crevice volumes (*e.g.* piston top-land, valve seats and injector well...) represents one of the major sources of HC emissions in gasoline Spark-Ignition (SI) engines for both direct and port-fuel injected SI engines operating at stoichiometric equivalence ratios. Fuel trapping in crevice volumes is particularly susceptible where early direct injection strategies are adopted since the in-cylinder pressures are relatively low and there is significant time available for fuel spray dispersion towards the walls of the cylinder liner. The potential contribution of HC emissions arising from the piston top-land crevice volume has been investigated in the present study on the standard engine. This has been achieved by varying the piston top-land configuration so as to increase the top-land crevice volume.

Another potential mechanism for HC emissions formation is through bulk quenching. In this case, quenching of the oxidation reactions can occur due to either excessively low temperature zones and/or significant variations in the local fuel equivalence ratio (*i.e.* the formation of locally over-lean or over-rich zones) within the combustion chamber. Temperature inhomogeneities can be induced for example by heat transfer between the in-cylinder charge and combustion chamber walls or by natural thermal inhomogeneities as a result of mixing within the bulk gases. Bulk quenching can therefore lead to premature extinction of the flame (or combustion zone). Any remaining unburned hydrocarbons within the combustion chamber formed as a result of incomplete oxidation reactions can subsequently be emitted into the exhaust gases. This formation mechanism of HC emissions is investigated in the present study by varying parameters such as the intake charge temperature and global equivalence ratio. Finally, wall wetting is another potential source of HC emissions in the case of direct injection engines. This phenomenon is particularly sensitive to combustion chamber geometry and injection timing. In conditions whereby excessive spray impingement results in the formation of liquid films, complete evaporation and oxidation of the fuel may not occur. The phenomenon of liquid film formation and its role as a potential source of engine-out HC emissions has also been investigated in the present study. On the all-metal engine, this was achieved via experiments in which fuels of differing volatilities were tested and on the optical access engine via in-cylinder tracer LIF imaging.

The objective of the present study was to attempt to identify, experimentally, the sources of HC emissions in a wall-guided, low temperature Diesel combustion system. This has been achieved through a combined approach using a single cylinder all-metal research engine and an optical access engine of similar geometry. In the latter case, laser-based diagnostic techniques enabled in-cylinder visualisation studies to be performed.

For the wall-guided combustion chamber geometry, Figure 1 shows the significant variation of HC emissions as a function of start of injection (SOI) timing. One of the

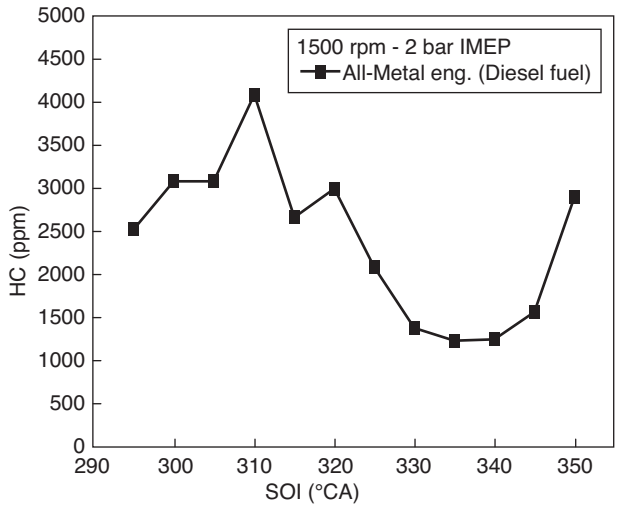

Figure 1

Variation of injection timing on HC emissions in a wall-guided, low NOx combustion system using high EGR rates, EGR = 45%, 2 bar IMEP, 1500 rpm (data obtained on all-metal engine).

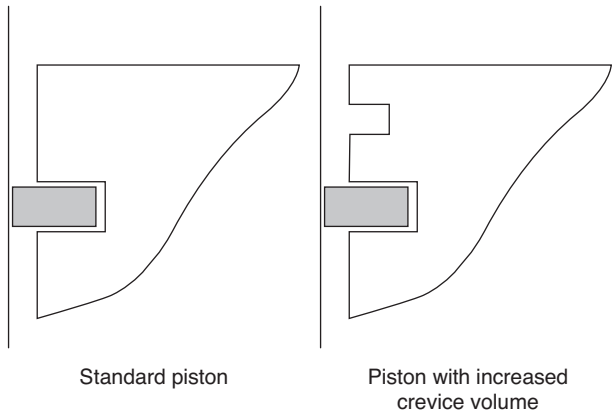

Figure 2

Schematic showing piston top-land geometry for standard piston (LHS) and piston with increased crevice volume (RHS) on all-metal engine.

primary objectives of the present study was to determine the causes for the trends observed in Figure 1. In addition to varying the SOI timing, parametric studies were performed in which variations of the intake charge temperature, equivalence ratio and engine coolant temperature were made.

INVESTIGATION METHODOLOGY

The potential sources of HC emissions, particularly for Port Fuel-Injected (PFI) or Direct-Injection (DI) gasoline engines are well documented [3]. As summarised briefly in the introduction, several of these "traditional" sources of HC emissions encountered in PFI or DI gasoline engines could be encountered in HCCI or low temperature Diesel combustion systems. As a result, suitable methodologies for investigating these possible sources have been explored and subsequently applied in the present study as follows:

– Crevice volumes: in order to determine the relative importance of the piston top land crevice volume as a source of HC emissions, experiments were performed on the all-metal engine using two piston heads. An additional groove was machined into one of the piston heads, within the piston top-land, just above the upper compression ring. Introducing this additional groove resulted in an increase of the top land crevice volume by a factor of two. A schematic diagram of the unmodified (*i.e.* standard piston) and modified (*i.e.* piston with increased crevice volume) piston heads is shown in Figure 2. The piston bowl volume was very slightly modified so as to maintain the same geometric compression ratio. This was achieved by reducing the bowl diameter by 0.5 mm (~1%) and the bowl depth by 0.2 mm (~1%). No other modifications were made to the form of the bowl dome or the re-entrant. These very minor modifications had no effect on the aerodynamic flow, mixture preparation and combustion characteristics. The piston-liner clearance was left unmodified so as not to favourably bias the entrainment of fuel into the top-land crevice volume. However, by adding the extra groove above the upper compression ring, it was possible to determine whether fuel enters this crevice volume during the engine cycle and assess the relative contribution (if any) of the trapped fuel on subsequent emission into the exhaust gases.

– Bulk quenching: in order to study the mechanism of bulk quenching which is believed to represent a significant source of HC emissions, the effects of varying parameters such as the equivalence ratio, start of injection timing and intake charge temperature were studied. The objective was to evaluate the role of bulk quenching and gain an insight in terms of the in-cylinder conditions which might be more susceptible to bulk quenching phenomena. For example, bulk quenching typically occurs under conditions in which local temperature and/or fuel concentration gradients exist. In-cylinder LIF imaging was performed on the optical-access engine which allowed the

detection of the spatial location of unburned HC, potentially providing complementary information on the bulk quenching mechanism.

– Jet impingement and liquid film formation: the influence of jet impingement and/or liquid film formation was investigated on the all-metal and optical-access engines. Since it has been shown from previous studies [7] that significant fuel spray-wall interaction occurs in the wall-guided chamber geometry, the potential for fuel film formation and the implications on HC emissions might be considerable. In order to study the role of fuel films on the all-metal engine, a so-called "multi-fuel" approach was adopted in which two fuels of different volatilities were tested. The objective was to isolate the phenomenon of fuel film formation (due to differences in fuel volatility). There then remains the question as to whether the use of a higher volatility fuel would introduce adverse effects on the mixture distribution. The authors believe this should not be the case since the mixture distribution is predominantly influenced by air entrainment and subsequent mass momentum transfer between the injected fuel and surrounding gas rather than effects related to fuel evaporation [9, 10]. Since the authors expect that fuel volatility effects on the vapour mixture distribution would be negligible, one can assume that any differences which might exist in terms of the HC emissions could be subsequently linked to liquid fuel film formation. However, in order to verify whether the effects of fuel volatility might influence the fuel distribution and ultimately as a step towards validating the "multi-fuel" approach used here, preliminary tests were performed using both fuels in a conventional Diesel combustion chamber geometry. These tests were performed using standard, wide angle spray nozzles where spray wall interaction is expected to be minimal in comparison to the wall-guided geometry. Complementary studies were also carried out on the optical-access engine using a tracer LIF technique which enabled the visualisation of liquid fuel films in the post-combustion gases. It should be noted that the tracer LIF experiments were performed for the wall-guided geometry only.

1 EXPERIMENTAL

1.1 Description of Optical and All-Metal Engines

Two single cylinder research engines were used in the present study. Studies of engine in-cylinder processes using laser-based optical diagnostic techniques were performed on an optically accessible engine whilst parametric studies were carried out on an all-metal (*i.e.* non-optical) version of the same engine. The major differences between the two engines are discussed briefly in this section. First of all, the reader should note that optical engines are devoid of a lubricating oil film between the cylinder liner and the piston rings. Furthermore, piston head cooling which is achieved by an underside oil jet on the all-metal engine is not implemented on the optical engine. It should also be noted that the piston top land crevice volume is greater in the case of the optical engine. This is as a result of lowering the piston ring pack on an optical engine so as to avoid overlap of the rings at the interface between the cylinder liner and the transparent sapphire crown. The top ring land crevice volume is taken into account in calculating the geometric compression ratio. Another difference between the two engines is that the piston heads are manufactured from different materials. In the case of the all-metal engine, the piston head material is aluminium whilst for the optical engine, the piston head is a two-piece arrangement. The major part is manufactured from titanium in order to minimise weight (and therefore inertia of the piston head/extended piston assembly). The base of the piston bowl allows either a transparent quartz window to be installed when optical access is required or an all-metal (in our case, steel) insert to be used if optical access is not needed. The differences in material properties could potentially have an effect on the combustion characteristics and emissions, these effects are discussed in more detail in the results section later in the paper. Finally, another significant difference between the two engines is the composition of the recycled exhaust gases used for charge dilution. On the all-metal engine, Exhaust Gas Recirculation (EGR) is achieved via an EGR loop which feeds EGR gases back into the intake air stream. The main constituent gases contained within EGR are the diatomic molecules CO_2 and H_2O in addition to N_2 and any remaining O_2 depending upon the operating condition. However, due to thermal constraints of the optical windows, it was not possible to operate the optical-access engine using real EGR since a skip-firing strategy was necessary. As a result, charge dilution on the optical engine was achieved via simulated EGR using N_2 as the principal diluent. The nitrogen was mixed upstream of the engine with the intake air. The flow rates of both air and nitrogen were controlled by means of sonic flow nozzles. The two intake gases were fed into the intake system well upstream (approximately 4 meters) of the engine thus ensuring a homogeneous air-nitrogen intake stream. The proportions of air and N_2 were controlled in order to obtain the required O_2 concentration. Engine data presented in this paper were taken at speeds of 1200 or 1500 rpm. Prior to data acquisition, the engine was preheated (oil and water "coolant" circuits) to 90°C. A summary of the engine specifications are provided in Table 1.

The all-metal and optical access engines had a geometric compression ratio of 14:1. Both engines were equipped with common rail fuel injection systems (Bosch) which are capable of supplying fuel at nominal rail pressures up to 1600 bar. A six-hole injector nozzle with a 60° included angle was used for all experiments on the wall-guided combustion geometry. As indicated in Table 1, the swirl ratio for the

TABLE 1

Engine specifications of the optical and all-metal engines

	All-metal engine	Optical engine
Engine base type	2 litre, DI Diesel	2 litre, DI Diesel
Number of cylinders	1	1
Number of valves	2 int. + 2 ex.	2 int. + 2 ex.
Bore/stroke	85/88 mm	85/88 mm
Displacement volume	0.5 l	0.5 l
Squish height	0.90 mm	1.13 mm
Piston crevice vol.	0.41 cm^3	0.94 cm^3
Compression ratio	14	14
Intake pressure	1 bar (abs.)	1 bar (abs.)
Swirl ratio	1.1	2.2

optical and all-metal engines were 2.2 and 1.1 respectively. Although the swirl level has been shown to significantly influence HC emissions for some low temperature Diesel combustion systems [11], this was not observed to be the case in the present study (these results will be presented in a future publication). For the tests performed on the all metal engine using a conventional Diesel engine combustion chamber geometry, a six-hole injector nozzle with a 152° included angle was used. As mentioned above, these tests were conducted so as to validate the "multi-fuel" approach used for the study of liquid fuel films. In-cylinder pressure measurements were acquired using a water-cooled piezoelectric pressure transducer (Kistler 6043A60). Pressure data obtained over 200 engine cycles were averaged in order to perform a 0-D combustion analysis and thus obtain parameters such as heat release rate, burned mass fraction and cycle temperature. An optical crank angle encoder with a resolution of 0.1 CAD was used. Both engines were equipped with an intake heater allowing pre-heating of the fresh intake air (or in the case of the optical access engine, the air-nitrogen mixture under simulated EGR conditions). The all-metal engine was equipped with an EGR line which incorporated a heat exchanger thus allowing cooled EGR gases to be fed into the intake air stream.

1.2 Study of Liquid Fuel Films

1.2.1 Multi-Fuel Approach

As described earlier in the paper, the presence of liquid fuel films and their potential impact on engine-out HC emissions was studied via a combination of optical diagnostics and a "multi-fuel" approach. In the latter case, two fuels were tested on the all-metal engine: a standard Diesel fuel and a higher volatility Fischer Tropsch/kerosene blend. The blend of 90% kerosene and 10% of a Fischer Tropsch fuel was formulated so as to maintain a similar cetane number compared to the standard Diesel fuel. The objective here was to perform engine tests using two fuels of varying volatility which might enable us to identify the significance of fuel film formation as a source of HC emissions. Furthermore, as described in the following sub-section, tracer-LIF imaging experiments performed on the optical access engine were carried out using dodecane fuel and 5-nonanone tracer (1% by mass). This fuel was also representative of a high-volatility fuel since the boiling point of dodecane (216°C) is at the lower end of the distillation curve of standard Diesel fuel (typical boiling points of Diesel fuel are in the range 175 to 350°C). The fuel properties are summarised in Table 2.

1.2.2 Visualisation of Liquid Fuel Films via Tracer LIF

In-cylinder imaging of liquid fuel films was performed via tracer LIF. In the present study, the objective was to determine whether liquid fuel films are formed on the piston surfaces for the wall-guided chamber geometry since it is known that

TABLE 2

Fuel specifications of the standard Diesel fuel, kerosene/Fischer Tropsch fuel blend and dodecane used in experiments on the all-metal and optical access engine

	Standard Diesel	Kerosene/FT blend	Dodecane
Sulphur (by weight)	44 ppm	-	-
Distillation temperatures			
Initial boiling point	173°C	194°C	216°C
10% distillation temperature	200°C	199°C	-
50% distillation temperature	272°C	219°C	-
90% distillation temperature	331°C	257°C	-
Final boiling point	352°C	297°C	216°C
Cetane number	51	51	80
Lower heating value	46.11 MJ/kg	46.53 MJ/kg	47.39 MJ/kg

significant spray-wall interaction occurs [7, 13]. In particular, the temporal evolution of liquid fuel films throughout the cycle was studied in order to assess whether these films may contribute to engine-out HC emissions. Since the objective was to detect the potential presence of liquid films at the end of combustion, it was crucial that the tracer LIF technique used in this study could be applied under reacting (*i.e.* combusting) conditions. The selected tracer should therefore have limited sensitivity to oxygen quenching under such conditions. This is in general a major limitation of many LIF tracers commonly used for in-cylinder visualisation studies. The selected tracer used in this study was 5-nonanone [14] since previous experiments in a high pressure, high temperature pre-combustion chamber have shown this tracer to be particularly suitable for imaging of combusting Diesel jets [15]. A small quantity (1% by mass) of 5-nonanone was added as a dopant to the single component (non-fluorescent) fuel dodecane.

Laser-induced fluorescence (LIF) of the tracer was achieved by excitation using a frequency-quadrupled Nd:YAG laser (266 nm). The output beam was diverged using a spherical lens producing a cone of light (*i.e.* flood illumination) which entered the combustion chamber via the 45° mirror (housed within the extended piston) and the large quartz piston bowl window *(Fig. 3)*. As a result, images obtained of the liquid film are integrated along the line-of-sight. A dichroic mirror allowed retro-collection of the LIF images onto an intensified CCD camera *(Roper Scientific, PIMAX)* equipped with a 105 mm objective lens (f/2.8). The camera gate (exposure) time was maintained constant at 50 ns for all LIF experiments. A combination of optical filters which enabled collection of the LIF emission in the spectral range 320 to 400 nm was used. These filters enabled efficient collection of the 5-nonanone fluorescence whilst minimising potential interference from combustion luminosity which is particularly intense (principally due to soot incandescence) in the visible wavelength spectral range.

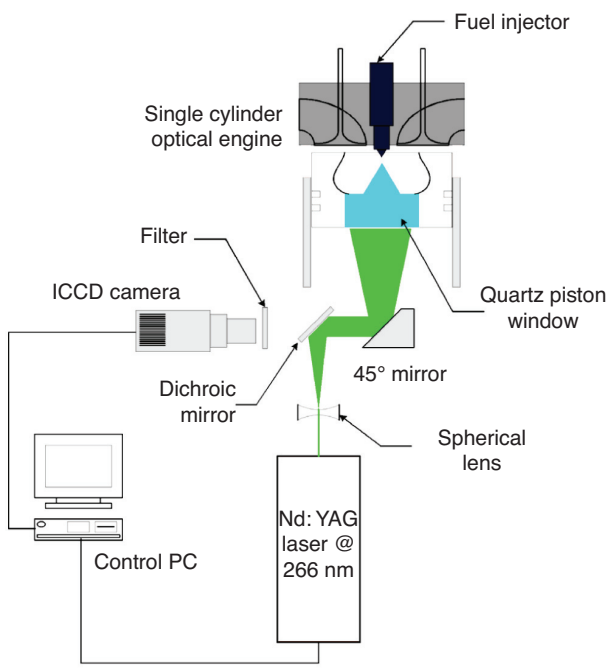

Figure 3

Schematic of the tracer LIF imaging setup used for visualisation of liquid fuel films on the optically accessible engine.

1.3 Study of HC Formation

Visualisation of Unburned HC via LIF Imaging

Laser-based diagnostics were applied for the study of HC emissions formation in the optical engine. Figure 4 shows a schematic of the optical access provided for the LIF imaging set-up used in this study. A fully transparent sapphire crown allowed in-cylinder visualisations just below the cylinder head whilst a large piston base quartz window enabled optical access inside the piston bowl. The optical engine measurements were performed using a skip-firing sequence of 1/5 (*i.e.* 1 fired cycle followed by 4 motored cycles). This skip-firing sequence was imposed so as to minimise thermal gradients across the optical windows. However, this operating mode also ensured the admission of fresh intake gases by eliminating any possible effects of trapped exhaust gas residuals from previous engine cycles thus providing well-defined in-cylinder conditions at bottom dead centre (BDC).

For LIF imaging of in-cylinder HC, the output beam of a frequency-tripled Nd:YAG laser (*i.e.* excitation wavelength of 355 nm with 50 mJ laser energy per pulse) was formed into a two-dimensional vertical sheet (15 mm height, 0.5 mm thickness) which traversed the engine cylinder via the fully transparent sapphire crown *(Fig. 4)*. The laser sheet provided access within a vertical plane below the cylinder head and coincident with the cylinder axis of symmetry for the detection of unburned HC within the squish zone in addition to the central part of the cylinder below the injector nozzle. The LIF images were collected at 90° via the transparent sapphire crown onto an intensified CCD camera. A 390 nm high pass optical filter combined with a 465 nm band pass filter (70 nm FWHM) were used to capture the LIF signal corresponding to unburned HC. Since standard Diesel fuel was used for these LIF experiments, laser excitation at a wavelength of 355 nm allowed detection of either intermediate species (formed as a result of fuel decomposition) such as formaledehyde, CH_2O [7, 12] or the natural fluorescence of any remaining unburned fuel[1] which has not been consumed during the main combustion process.

1 Commercial Diesel fuels typically contain aromatics and napthenes which are efficient fluorescence emitters following UV excitation.

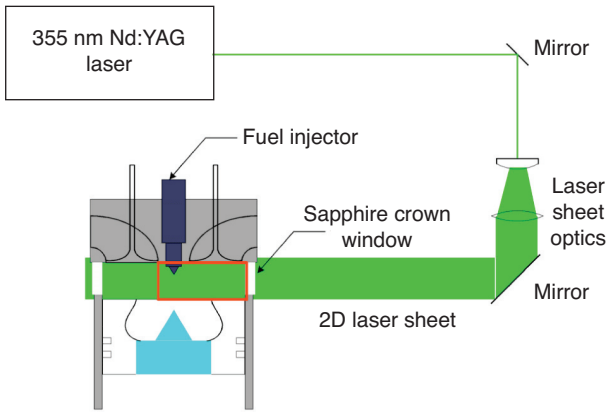

Figure 4

Schematic of the LIF imaging setup used for visualisation of in-cylinder unburned HC on the optically accessible engine. Images were collected at 90° via the sapphire crown window. An outline of the imaged area is indicated by the red line.

In order to optimise LIF image signal-to-noise ratio, it was particularly important to ensure accurate alignment of the laser sheet so that it traversed the transparent sapphire crown coincident with the axis of symmetry. Slight deviations of the laser sheet otherwise resulted in significant optical noise due to internal laser sheet reflections. Furthermore, it was necessary to mask a small zone in front of the injector nozzle to avoid image saturation as a result of elastic laser sheet scattering. The rectangular masked zone is indicated by a white outline in the LIF images presented later in the paper.

2 RESULTS

The results presented in this paper, obtained via experiments performed on the all-metal and optical-access engines, are discussed in three subsequent sections corresponding to the principal mechanisms of HC emission which have been investigated during the course of this study (*i.e.* bulk quenching, liquid films and crevice volumes). Since this study was based on a combined approach using a standard, all-metal and an optical-access engine, initial experiments were carried out in order to compare the two engines in terms of combustion behaviour and engine-out emissions and establish whether the two engines respond similarly to variations of parameters such as SOI timing and charge dilution. For these preliminary experiments, the optical-access engine was operated in an "all-metal" configuration (*i.e.* all optical/transparent windows were replaced by identical metal inserts). The optical engine was operated with standard Diesel fuel and without skip-firing. Experiments were then performed on both engines for a similar range of operating conditions. An analysis of the experimental data (*i.e.* in-cylinder pressure, heat release rate and measured engine-out emissions) thus enabled a comparison of the two engines. The results of these experiments are discussed in the following sub-section.

2.1 Comparison of Optical and All-Metal Engine

Preliminary engine experiments were carried out to enable a comparison between the all-metal and optical-access engines in terms of combustion behaviour (*e.g.* combustion phasing) and the engine out HC emissions for varying SOI timings and levels of charge dilution. A comparison of in-cylinder pressure data obtained for the two engines is shown in Figure 5 for a global equivalence ratio (ϕ) of 0.22. This engine operating condition, in the absence of EGR enables a comparison of the combustion phasing for the two engines whilst eliminating any possible effects that may arise from differences in intake charge composition (*i.e.* the effects of real EGR versus simulated EGR). The reference case, corresponding to the pressure trace for the all-metal engine is for a SOI timing of 340°CA (*i.e.* 20°CA before TDC), engine speed of 1500 rpm, IMEP of 2 bar and intake temperature of 60°C.

A comparison of in-cylinder pressure traces obtained on the optical-access engine for the same SOI timing (340°CA) reveals that combustion phasing is significantly advanced with auto-ignition occurring several crank angle degrees earlier compared to the all-metal engine.

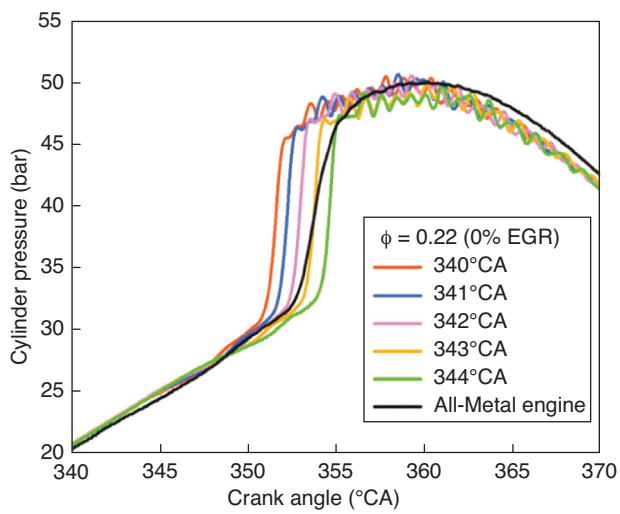

Figure 5

Comparison of in-cylinder pressure traces obtained for a SOI timing sweep on the optical engine and for SOI = 340°CA on the all-metal engine, ϕ = 0.22 (0% EGR), 1500 rpm, IMEP 2 bar, T_{int} = 60°C.

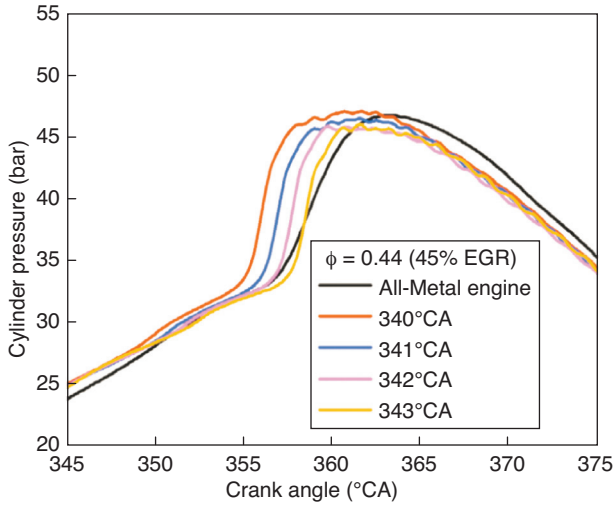

Figure 6

Comparison of in-cylinder pressure traces obtained for a SOI timing sweep on the optical engine and for SOI = 340°CA for all-metal engine, ϕ = 0.44 (45% EGR), 1500 rpm, IMEP 2 bar, T_{int} = 60°C.

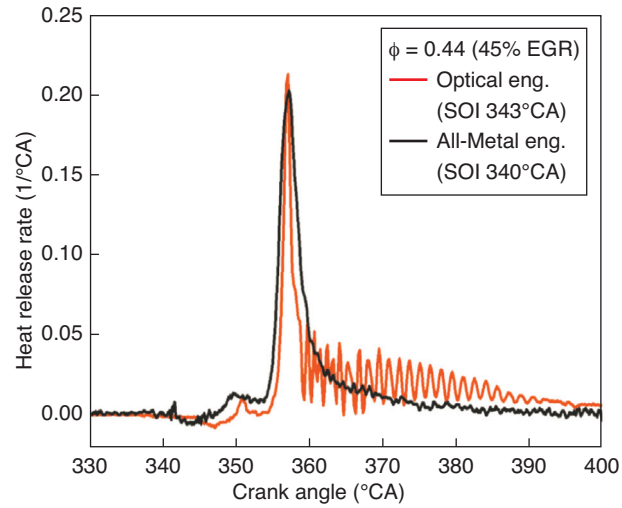

Figure 7

Comparison of heat release rates for the optical engine (SOI = 343°CA) and all-metal engine (SOI = 340°CA), ϕ = 0.44 (45% EGR), 1500 rpm, IMEP 2 bar, T_{int} = 60°C.

Furthermore, the pressure-rise rate is clearly higher on the optical engine. A subsequent sweep of the SOI timing in 1°CA increments shows that the auto-ignition timing can be phased correctly for a SOI timing of 343°CA however this is not an appropriate solution since it affects the mixture preparation (*e.g.* jet-wall impact location). Clearly, the auto-ignition delay is shorter in the case of the optical-access engine. The possible reasons for this are discussed later in the paper.

Figure 6 shows in-cylinder pressure traces obtained for an EGR rate of 45%. It is well known that increasing the level of charge dilution results in a longer auto ignition delay and a noticeable decrease in the pressure-rise rate (slower chemical kinetic reactions). These effects are shown by comparing the data of Figure 5 and Figure 6. Under dilute conditions (ϕ = 0.44), Figure 6 reveals that significant differences remain in terms of the combustion phasing when comparing the optical and all-metal engines for a SOI timing of 340°CA. As was shown in Figure 5, retarding slightly the SOI timing to 342/343°CA enables the start of combustion to be phased more accurately although the ignition delay is clearly much shorter in the case of the optical engine. A higher pressure-rise rate is also observed, indicating faster reaction rates.

A comparison of the heat release rates is shown in Figure 7 for the operating condition corresponding to 45% EGR (ϕ = 0.44). These data are shown for the SOI timing of 343°CA for the optical-access engine compared to the nominal SOI timing of 340°CA on the all-metal engine. The heat release data reveals that retarding the SOI timing by 3°CA on the optical engine allows a reasonably satisfactory agreement in terms of the "hot" auto ignition timing which occurs at approximately 355°CA. However, Figure 7 reveals that prior to the "hot" auto ignition, the cool-flame reactions (as indicated by the initial, smaller peak in the heat release rate) occur over a noticeably shorter period compared to the all-metal engine. This indicates faster chemical kinetics of the intermediate "pre-combustion" reactions on the optical-access engine. Although the "hot" auto ignition timing is comparatively well phased between the two engines by slightly retarding the SOI timing on the optical engine, the subsequent heat release rate appears to be slightly higher (as indicated by the gradient of the main heat release) for the optical engine whilst the combustion duration is also noticeably shorter compared to the all-metal engine.

The data presented above revealed noticeable differences in terms of the combustion phasing and pressure rise rates between the optical and all-metal engines. However, it was also necessary to compare the engine-out HC emissions behaviour and in particular to determine whether the trends observed in Figure 1 are comparable for both engines. The effects of SOI timing on HC emissions are shown in Figure 8 for the all-metal and optical access engines. Experiments on the optical access engine enabled a comparison to be made between standard Diesel and

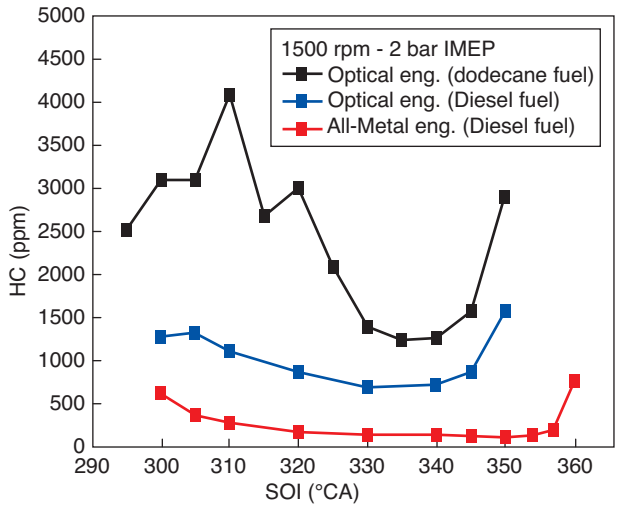

Figure 8

Variation of SOI timing on HC emissions for optical access engine using standard Diesel and dodecane fuel, EGR = 45%, 2 bar IMEP, 1500 rpm, T_{int} = 60°C.

dodecane fuels and their impact on engine-out HC emissions. Figure 8 reveals that for standard Diesel fuel, measured HC concentrations were significantly lower (approximately 2 to 2.5 times lower) on the optical engine compared to the all-metal engine for a SOI timing sweep between 300 and 360 °CA. Despite significant differences in the levels of unburned HC, Figure 8 confirms that the trends observed are quite similar: For early SOI timings, between 300 and 320°CA, relatively high levels of HC are detected. As SOI timing is progressively retarded later into the compression stroke, the concentration of unburned HC decreases to a minimum corresponding to a SOI timing of approximately 340°CA. Thereafter, the HC emissions rapidly increase for even later SOI timings closer to TDC.

As discussed earlier, dodecane fuel which is commonly used as a surrogate "Diesel" fuel for LIF experiments on optical engines has a much higher volatility compared to standard Diesel. The HC emissions data shown in Figure 8 clearly reveal that the use of dodecane fuel leads to even lower levels of HC emissions compared to standard Diesel fuel. This result is perhaps not surprising since fuel evaporation would be enhanced due to the lower boiling point of dodecane. Furthermore, the shape of the curve showing the evolution of the HC emissions with SOI timing shows noticeably less variation for dodecane fuel compared to Diesel fuel. In summary, the results presented in Figure 8 tend to confirm that the use of dodecane fuel for the optical engine studies would be somewhat misleading since the sensitivity and behaviour of the HC emissions to SOI timing is not as well reproduced compared to the use of standard Diesel fuel. Consequently, it was decided that subsequent in-cylinder LIF visualisations on the optical engine for the study of HC emissions sources would be performed using standard Diesel fuel in order to maintain comparable trends as much as possible between the two engines. Liquid film visualisations performed via the tracer LIF technique required the use of a pure, non-fluorescing base fuel (dodecane) which was doped with a small quantity of 5-nonanone tracer.

2.2 Crevice Volumes in Wall-Guided Geometry

The role of combustion chamber crevice volumes as potential sources of unburned HC emissions in the wall-guided system was investigated on the all-metal engine. Previous studies reported in References [1, 2] were performed on an HCCI engine operating in fully premixed mode with intake air heating. Results from those particular studies revealed that unburned fuel from crevice volumes represented a significant proportion of the engine-out HC. The present study however focuses on a direct-injection, Diesel-fuelled engine operating under HCCI-like conditions (*i.e.* low temperature combustion to achieve low NOx and particulate emissions) with a fully representative combustion chamber geometry. A groove was introduced between the piston top surface and the first piston ring as indicated by the schematic diagram shown earlier in Figure 2. The groove volume was calculated so as to increase the topland crevice volume by a factor of two. Furthermore, in order to maintain the same compression ratio (14:1) between the two combustion chamber geometries, the piston bowl volume was very slightly reduced in the case of the piston with groove whilst maintaining the same form so as not to influence the mixture preparation (location of jet impingement, fuel jet trajectories, etc.).

A comparison of the measured HC emissions for a SOI timing sweep is shown in Figure 9. The results, obtained on the all-metal engine show that increasing the piston topland crevice volume has a negligible effect on the level of engine-out HC emissions over a wide range of SOI timings. These findings seems to correspond well with the in-cylinder LIF imaging data obtained on the optical engine. The visualisations performed using the LIF technique did not reveal an marked presence of unburned HC in the vicinity of the liner which might otherwise indicate fuel being drawn out of the topland crevice volume. It was therefore concluded that the piston top land crevice volume has a negligible effect on the engine-out HC emissions for the wall-guided chamber geometry.

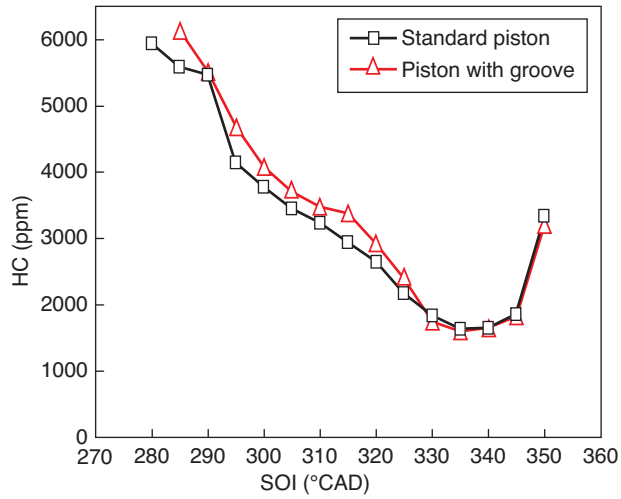

Figure 9

Comparison of HC emissions levels as a function of SOI timing showing effect of piston topland crevice volume, IMEP 4 bar, 45 %EGR, 1500 rpm, T_{int} = 60°C, all-metal engine data, wall-guided geometry.

2.3 Bulk Quenching

2.3.1 All-Metal Engine Results

The influence of intake charge temperature and equivalence ratio on HC emissions were investigated on the all-metal engine at an engine speed of 1500 rpm and for two low load conditions (2 and 4 bar IMEP). For the 2 bar IMEP condition, the intake charge temperature was varied in the range 40 to 95°C whilst the equivalence ratio was varied in the range 0.2 to 0.45. For the 4 bar IMEP operating condition, the equivalence ratio was varied in the range 0.32 to 0.8. The equivalence ratio was varied by altering the EGR rate whilst maintaining a constant intake manifold pressure. The intake charge temperature (measured within the intake manifold just above the intake valves) was varied by regulating the intake air temperature using a heater installed upstream of the intake port. The maximum cycle temperature was calculated via a 0D combustion analysis [3] using the in-cylinder pressure data. This analysis is based on the assumption that the combustion chamber temperature is uniform which is in general not the case since it has been shown that natural charge and thermal inhomogeneities tend to exist in HCCI combustion [13, 16, 17]. However, the analysis is nonetheless useful since it enables at least a comparative study for the various engine operating conditions and in particular the effect of equivalence ratio on engine-out HC emissions. The influence of intake charge temperature on engine-out HC emissions is shown in Figure 10 (upper graph) for various equivalence ratios in the range 0.20 to 0.45.

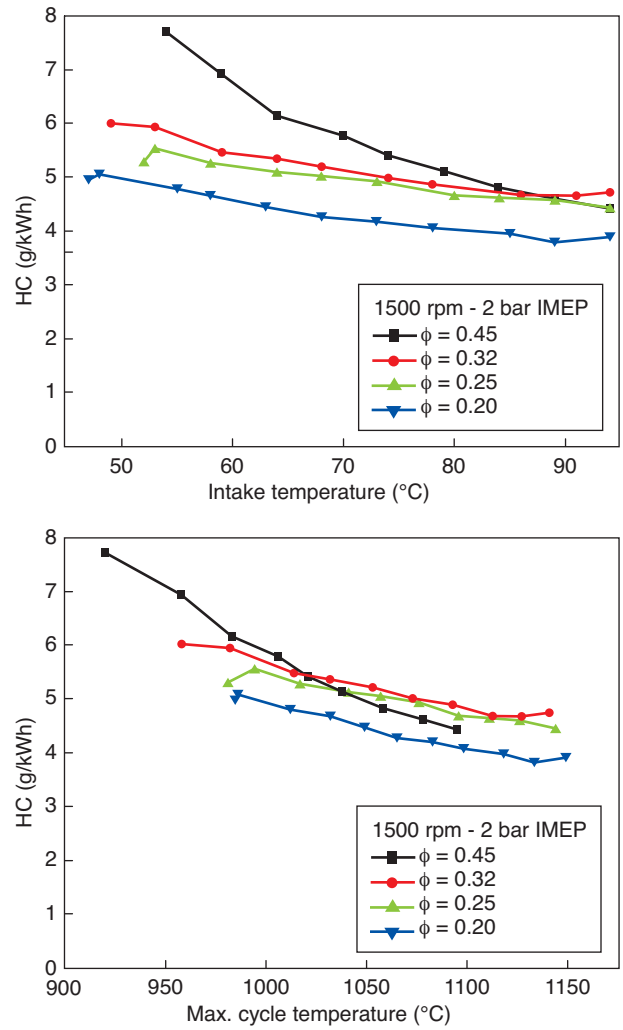

Figure 10

Variation of HC emissions levels as a function of intake charge temperature (upper graph) and maximum cycle temperature (lower graph) for a range of equivalence ratios, SOI 340 CAD, 1500 rpm, 2 bar IMEP.

The results show that an increase in the intake charge temperature leads to a systematic decrease in the level of HC emissions for the range of equivalence ratios studied. Furthermore, one observes that at relatively high intake temperatures (in excess of 85°C), the HC emissions levels converge to very similar values for equivalence ratios in the range 0.25 to 0.45 whereas for the lowest equivalence ratio, 0.2, the measured HC emissions are consistently lower. At iso-intake temperature, the upper graph of Figure 10 reveals that the level of HC emissions is clearly influenced by the equivalence ratio, with a notable increase in the HC emissions for high equivalence ratios (*i.e.* increasing

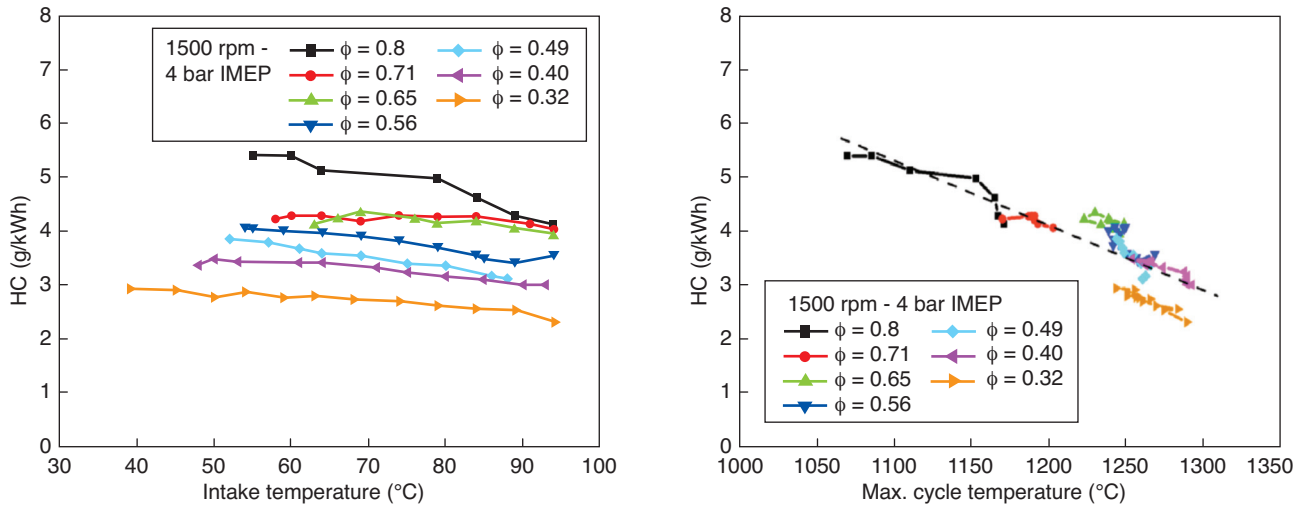

Figure 11

Variation of HC emissions levels as a function of intake charge temperature (upper graph) and maximum cycle temperature (lower graph) for a range of equivalence ratios, SOI 340 CAD, 1500 rpm, 4 bar IMEP.

charge dilution). The beneficial effect as a result of an increase in the maximum cycle temperature (in terms of reducing the HC emissions) is even more noticeable at the highest equivalence ratio condition ($\phi = 0.45$).

The HC emissions levels are also plotted as a function of peak or maximum cycle temperature (lower graph of *Fig. 10*). The results show that the highest levels of HC emissions are attained for the highest equivalence ratios whilst an increase in the intake temperature and peak cycle temperature correlate with a systematic reduction of the HC emissions. Furthermore, in the range of equivalence ratios 0.25 to 0.45, the level of unburned HC appears quite comparable for a given peak cycle temperature, *i.e.* the equivalence ratio appears to have relatively little effect on the level of HC emissions (except for the lowest equivalence ratio of 0.20). Indeed, the peak cycle temperature appears to have a first order effect in determining the HC emissions levels. Engine data was also obtained at a slightly higher load condition corresponding to an IMEP of 4 bar *(Fig. 11)*.

The upper graph of Figure 11 reveals that an increase in the intake charge temperature does not have a significant effect on the engine-out HC emissions levels except for the highest equivalence ratio of 0.8. In contrast however, the HC emissions reveal a systematic decrease with an increase in the peak cycle temperature as shown by the lower graph of Figure 11. Furthermore, one observes that for a given equivalence ratio, a significant increase in the intake temperature (in general in the range 50 to 90°C) does not appear to have a significant effect on the maximum cycle temperature attained. This is certainly the case within the range of equivalence ratios for 0.32 to 0.71, although appears to be different for $\phi = 0.8$ corresponding to a very high level of charge dilution. These results therefore seem to confirm that the peak cycle temperature has a first order effect on the level of HC emissions (*i.e.* an increase in maximum/peak cycle temperature correlates with a reduction of the measured engine-out HC emissions). In contrast however, an increase in the equivalence ratio appears to result in a rather limited increase in HC emissions. This latter parameter thus seems to have a lesser effect on the level of HC emissions. The trend showing the correlation between HC emissions and maximum cycle temperature appears to be independent of the equivalence ratio in the range 0.4 to 0.8 and a linear fit can be applied to the data points which reveals a monotonic decrease in the HC emissions independent of the equivalence ratio. However, the data points corresponding to the lowest equivalence ratio of 0.32 (0% EGR) do not coincide with the linear curve approximation. The variation of HC emissions as a function of equivalence ratio and maximum cycle temperature is shown in Figure 12.

The data presented in Figure 12 summarises more succinctly the relative effects of equivalence ratio and maximum cycle temperature on the level of engine-out HC emissions. In particular, one observes that for a given maximum cycle temperature, varying the equivalence ratio seems to have a rather limited impact on the HC emissions. In contrast, for a given equivalence ratio, an increase in the maximum cycle temperature has a significant effect on the level of HC emissions. These data tend to confirm that the maximum cycle temperature is a first-order parameter in terms of its influence on HC emissions whilst the equivalence ratio appears as a second-order parameter.

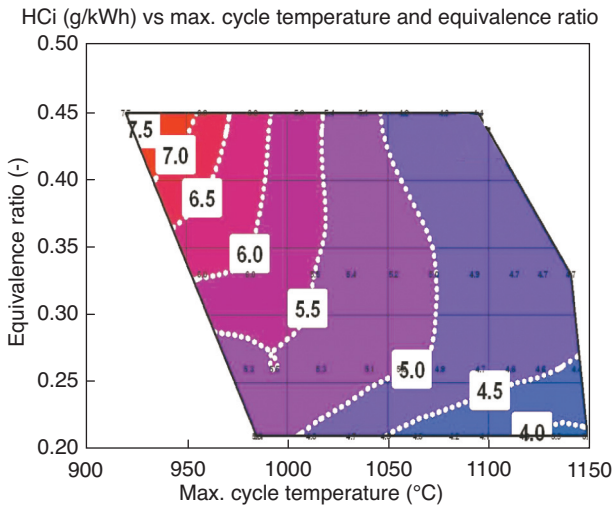

Figure 12

Engine-out HC emissions data as a function of the equivalence ratio and maximum cycle temperature, SOI 340 CAD, 1500 rpm, 2 bar IMEP.

2.3.2 Optical Engine Results – Variation of Intake Temperature

The effect of intake temperature on the formation of in-cylinder HC was also investigated using optical diagnostics. As explained earlier in the paper, standard Diesel fuel was used for these experiments since the use of a higher volatility "pure" fuel such as dodecane was found to have significant effects on the unburned HC emissions. Planar LIF imaging was performed with excitation at 355 nm allowing the detection of either intermediate products formed as a result of fuel decomposition (*i.e.* unburned oxygenated HC compounds such as formaldehyde) or simply unburned fuel. The LIF technique is useful as it provides a qualitative[2] insight of the location of in-cylinder HC and might thus give an indication as to the potential mechanisms of HC formation (*i.e.* HC arising from crevice volumes, HC detected in the bulk gases...). Furthermore, the intensity of the LIF signal provides at least a comparative indication of the level of in-cylinder HC, for example in response to a parametric variation (*e.g.* intake temperature, SOI timing, charge dilution, etc.).

The detection of in-cylinder unburned HC via LIF imaging is not straightforward. Firstly, a comparison of the measured HC emissions for the all-metal and optical-access engines *(Fig. 8)* revealed significantly lower levels of unburned HC in the case of the optical engine. As a result, the subsequent detection of such low in-cylinder concentrations (several hundred ppm) via LIF imaging proved to be even more challenging since detection is only possible within a single, vertical plane illuminated by the laser sheet. Secondly, HC emissions are generally problematic at low engine load conditions and it is under such conditions that HCCI combustion stability is limited. As a result, particular care was required when interpreting the LIF data since the detected signal, indicating the presence of in-cylinder HC could be formed as a result of quenching in the bulk gases under normal engine firing conditions. However, high concentrations of unburned HC species will also be detected for cycles corresponding to partial burn or complete cycle misfires. It was thus necessary to acquire simultaneously the in-cylinder pressure trace with the corresponding LIF image. To illustrate this, Figure 13 shows single-shot LIF images of in-cylinder HC observed from four separate cycles. The corresponding in-cylinder pressure traces for the LIF images of Figure 13 are shown in Figure 14. The ensemble-averaged pressure curve (in black), acquired over 200 consecutive engine cycles is compared with four single-cycle pressure traces corresponding to the four single-shot LIF images of unburned HC shown in Figure 13.

The single-cycle pressure traces immediately reveal that cycle 22 corresponds to an engine cycle "misfire". Interestingly, the initial drop in cylinder pressure that typically follows fuel injection (due to intake charge cooling as a result of fuel evaporation) is not observed for cycle 22. Subsequently, combustion does not occur during this cycle although a slight bump in the pressure trace after 365 CAD suggests that subsequent post oxidation of a quantity of the injected fuel may have occurred. For cycles 17, 20 and 48, the acquired pressure data does not indicate any abnormality

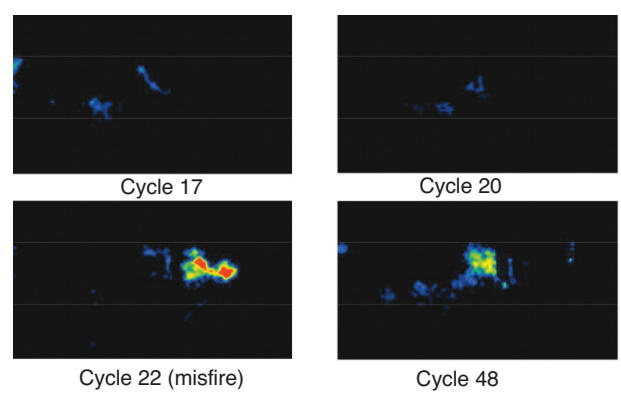

Figure 13

Comparison of single-shot LIF images of in-cylinder unburned HC in the post-combustion gases of the wall-guided chamber geometry, images acquired at 430 CAD, EGR = 45%, 2 bar IMEP, SOI 340 CAD, T_{int} = 60°C.

2 The LIF studies performed here are purely qualitative since the fluorescing species have not been identified. Furthermore, the dependencies of their LIF signals on pressure, temperature and mixture composition (collisional quenching effects) are unknown.

and combustion appears to occur as normal. The single-shot LIF images of Figure 13 reveal the presence of in-cylinder HC late into the expansion stroke (at 430 CAD) for all four cycles. As would be expected, the detected LIF signal intensity is significantly higher for cycle 22, indicating a higher concentration of unburned HC. However, an intense LIF signal is also observed for cycle 48, indicating the presence of in-cylinder HC even though the pressure data indicates that "normal" combustion occurs (*i.e.* no indication of a partial burn or complete cycle misfire). This particular example reveals the presence of unburned HC within the bulk gases and above all the importance of acquiring simultaneously the LIF images and in-cylinder pressure data to enable unambiguous interpretation of the LIF imaging data.

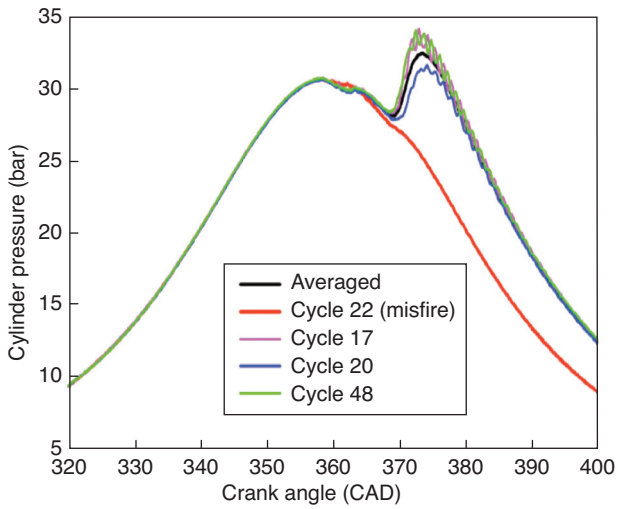

Figure 14

Comparison of single cycle in-cylinder pressure data acquired simultaneously with LIF images of unburned HC *(see images of Fig. 13)*.

LIF imaging was performed for various intake temperatures between 30 and 60°C in order to assess the effects on the spatial and temporal distribution of in-cylinder unburned HC. Sequences of ensemble-averaged LIF images acquired late into the expansion stroke and up until EVO are shown in Figure 15. The LIF images presented in Figure 15 show the extents of the optical access provided by the transparent sapphire crown (as indicated by the lower and upper white horizontal lines within the images). As explained earlier, it was necessary to place a mask in front of the CCD camera in order to avoid image saturation due to elastic scattering of laser light off the injector nozzle. The masked area within the image is shown by the rectangle within the upper left zone of the LIF images. Image corrections were made for background noise however spatial variations of laser sheet intensity were not accounted for.

Figure 15 reveals that for an intake temperature of 30°C, the spatial distribution of the LIF signal is relatively homogeneous, indicating the likely presence of unburned species within the central region of the cylinder and extending out

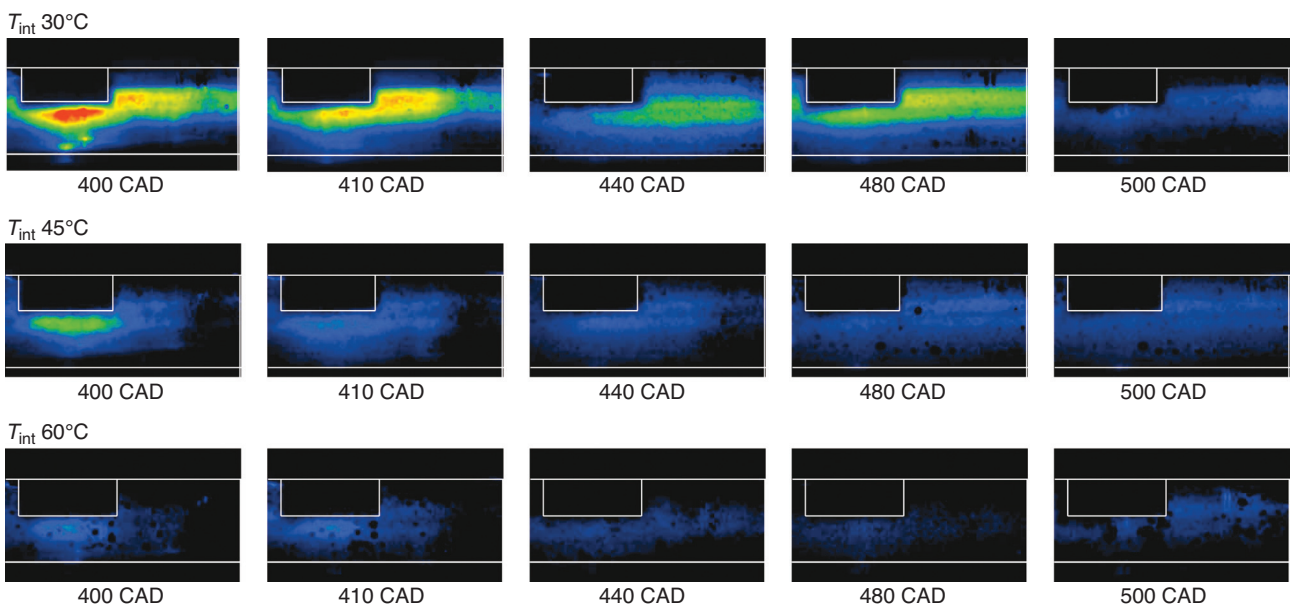

Figure 15

Comparison of ensemble-averaged LIF image sequences of in-cylinder unburned HC in the post-combustion gases of the wall-guided chamber geometry for various intake temperatures, EGR = 45%, 2 bar IMEP, SOI 340 CAD.

towards the liner. The LIF image intensities are initially quite high the signal levels progressively decrease later in the expansion stroke. At 500 CAD, corresponding to EVO, the LIF signal intensity appears to have decreased quite considerably and this might be due to the combined effects of post oxidation of the remaining unburned fuel within the hot burned, bulk gases and a decrease in the in-cylinder density during the expansion stroke. However, a certain quantity of unburned HC is detected within the vertical plane illuminated by the laser sheet. Furthermore, the homogeneous distribution of the detected signal suggests that the unburned species are present within the mass or bulk gases rather than located within a particular zone within the combustion chamber. The results presented in Figure 15 also reveal that increasing the intake temperature progressively to 45 and then 60°C does not have a significant effect in terms of the spatial distribution of the LIF signal. At 400 and 410 CAD, a region of high LIF intensity is observed in the central part of the combustion chamber. The presence of HC in this zone of the combustion chamber might be due to unburned species which were previously located within the piston bowl and which are subsequently drawn out into the engine cylinder during the expansion stroke. The most notable effect of increasing the intake temperature is that one observes a progressive decrease in the overall LIF signal levels, whilst the spatial distribution of the unburned species appears to remain unchanged. Increasing the intake temperature, which has previously been shown to correlate with an increase in the maximum cycle temperature, seems therefore to lead to a reduction in the overall concentration of in-cylinder unburned HC. The fact that the spatial location of the LIF signal appears to remain unchanged tends to suggest that the phenomenon or mechanism responsible for HC formation in this case is similar (*i.e*. the LIF signal levels decrease within the bulk gases globally). These observations appear to show that the effect of higher intake temperatures (and therefore higher maximum cycle temperatures) which leads to a noticeable reduction in the level of in-cylinder HC is potentially linked to bulk-quenching. Furthermore, the results obtained via LIF imaging tend to corroborate the data obtained on the all-metal engine which previously showed that higher intake temperatures systematically result in lower levels of HC emissions. As discussed earlier in the paper, this is believed to be due principally to the beneficial effects of higher maximum cycle temperatures which allow the hydrocarbon oxidation reactions to go to completion.

2.3.3 Optical Engine Results – Variation of SOI Timing

The influence of injection timing on the location of in-cylinder HC was also investigated via LIF imaging. In particular, late SOI timings near to top dead centre (TDC) were studied. Under such SOI conditions, significant spray-wall interaction is known to occur for the wall-guided combustion chamber geometry used in the present study. The narrow angle direct injection (NADI) piston geometry is designed to optimise the fuel jet trajectories under late SOI timings via interaction with the bowl-dome and the re-entrant bowl wall so as to enhance air-fuel mixing and fuel evaporation [7]. LIF image sequences are shown in Figure 16 for SOI timings at 354, 356 and 358 CAD (360 CAD corresponding to TDC). For a SOI timing at 354 CAD, the LIF images reveal the presence of HC in the central part of the cylinder (note that the piston is below the camera field of view during the expansion stroke). An absence of LIF signal in the vicinity of the cylinder wall suggests that HC is not present in the squish zone (at least within the plane illuminated by the laser sheet). This is due to the fact that for late SOI timings, fuel is confined within the piston bowl due to the narrow spray angle and fuel guiding effect as discussed previously in References [7, 13]. Clearly, the LIF signal levels are very low, indicating comparatively low concentrations of HC and remains preferentially located in the central region of the cylinder until approximately 460 CAD. At 500 CAD, corresponding to Exhaust Valve Opening (EVO) the LIF signal levels reduce to negligible levels suggesting that HC is either absent in this zone or that the concentration of HC is too low to be detected. Retarding the SOI timing by 2 CAD does not appear to have an effect on the spatial location of HC. As was observed for the SOI timing at 354 CAD, the LIF signal indicates the presence of HC predominantly within the central region of the cylinder. At 500 CAD corresponding to exhaust valve opening, the acquired LIF signal, although relatively weak, reveals the presence of in-cylinder HC in a zone which extends out from the central zone towards the cylinder liner. The data suggests that the level of in-cylinder HC increases with retarding injection timing. This trend is further emphasised by retarding the SOI timing to 358 CAD.

As shown by the in-cylinder pressure data *(Fig. 17)*, the SOI timing of 358 CAD results in excessively retarded combustion phasing and an associated loss of combustion stability. Clearly, the combined effects of low in-cylinder pressure and temperature ensure that the oxidation reactions do not go to completion prior to piston volume expansion. Retarding the SOI timing from 354 to 358 CAD leads to a notable increase in the LIF image signal-to-noise ratio, indicating a higher concentration of in-cylinder HC although the spatial distribution of the unburned HC does not appear to evolve significantly. Although the SOI timing at 358 CAD does not correspond to an optimised engine operating condition, progressively retarding the SOI timing enables a comparative analysis of the spatial location of in-cylinder HC which can prove useful for identifying the possible formation mechanism. Indeed, the LIF images shown in Figure 16 corresponding to the SOI timing at 358 CAD reveal that the spatial location of in-cylinder HC is comparable with the 354 and 356 CAD SOI timings at 400 CAD. The most intense region is observed in the central zone of the cylinder at 400 CAD, probably due to the unburned fuel which exits

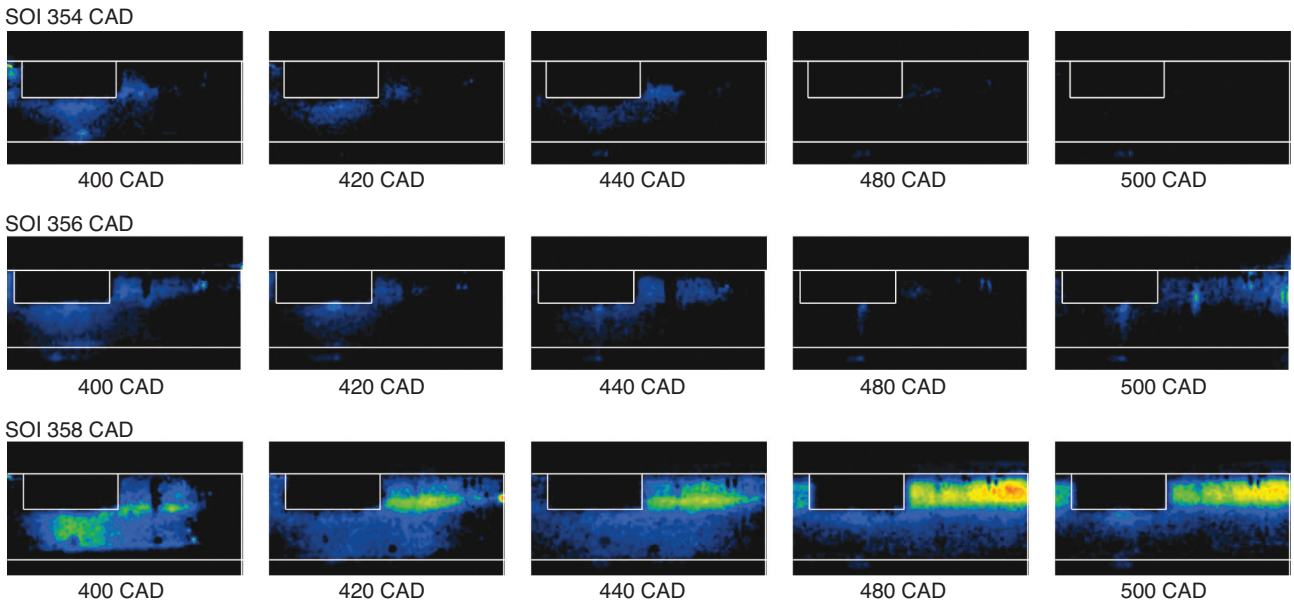

Figure 16

Comparison of ensemble-averaged LIF image sequences of in-cylinder unburned HC in the post-combustion gases of the wall-guided chamber geometry for late SOI timings, T_{int} = 60°C, EGR = 45%, 2 bar IMEP.

the piston bowl. Subsequently, significant LIF signal levels are observed in the region extending from the central part of the cylinder towards the liner wall, just below the cylinder head. It appears as though the dispersion of unburned HC is confined within the vicinity of the cylinder head, forming a locally rich zone in this region of the cylinder. Unburned fuel is detected at exhaust valve opening (500 CAD), and would then presumably be emitted into the exhaust gases.

A reasonable correlation is observed between the LIF imaging data obtained for these late SOI timings and the engine-out HC emissions trends as a function of SOI timing shown in Figure 1. As mentioned earlier, progressively retarding the SOI timing nearer to TDC eventually leads to a loss of combustion stability due to the excessively low in-cylinder pressures and temperatures which are attained. Quenching of the combustion reactions thus leads to a significant increase in the level of unburned HC (shown in *Fig. 1*) and it is believed that bulk quenching is one of the predominant mechanisms responsible for HC formation in this particular engine. Further discussion is provided in the following sub-section.

The LIF images acquired for the SOI timing at 358 CAD revealed the presence of what appears to be a significantly high concentration of unburned HC in the vicinity of the cylinder head late into the expansion stroke. A similar spatial distribution of the LIF signal was observed for the 356 CAD SOI timing although the signal-to-noise ratio was noticeably

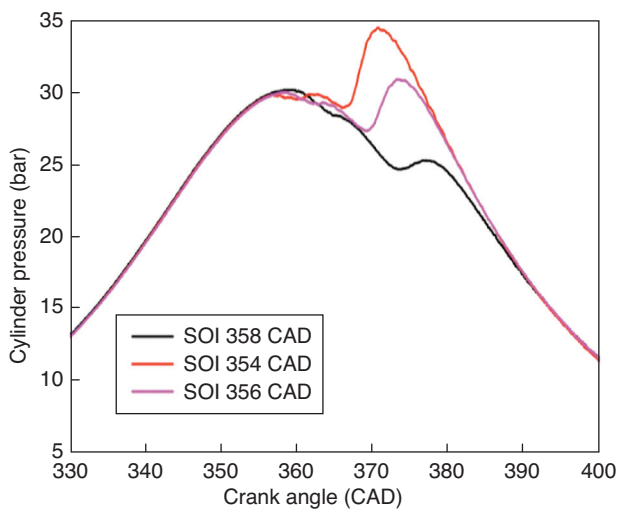

Figure 17

Comparison of ensemble-averaged in-cylinder pressure data showing effect of retarded SOI timing on combustion phasing, EGR = 45%, T_{int} = 60°C, 2 bar IMEP.

weaker. The authors believe that the presence of unburned HC in this region of the cylinder is inherently related to the mixture preparation process. In particular, it is known from previous investigations [7] that the adoption of late SOI timings (*i.e.* close to TDC) using the NADI combustion chamber

geometry has a significant effect on the fuel jet trajectories. As reported in [7], the form of the piston bowl dome and the re-entrant walls plays an important role on the fuel jet penetration and fuel-air mixing. The fuel guiding effect is, in general, beneficial in terms of improving mixture homogeneity. However, for very late SOI timings, it is believed that the fuel guiding effect occurs to such an extent that a significant quantity of the injected fuel is re-circulated upwards and outwards of the piston bowl via the re-entrant bowl wall. Subsequently, since the piston is near to TDC and thus in very close proximity to the cylinder head, further transport of the fuel mixture is prohibited. As such, the fuel mixture appears to stagnate in this zone just below the cylinder head. A schematic representation *(Fig. 18)* shows the probable fuel jet trajectory and subsequent formation of a fuel-rich (stagnation) zone. Although further air-fuel mixing may occur prior to combustion, primarily due to the bulk flow motion induced by the piston movement early during the expansion stroke, the degree of subsequent fuel dispersion throughout the cylinder is believed to be limited. The formation of a locally fuel-rich zone would likely result in incomplete oxidation of the fuel (*i.e.* undermixing effect). It therefore appears that in this case, the mechanism responsible for the unburned HC emissions is due to bulk quenching as a result of the formation (locally) of an over-rich fuel mixture and the consequent lack of available oxygen. This hypothesis would explain why a significant concentration of unburned HC is detected in the location below the cylinder head as shown by the LIF data of Figure 16.

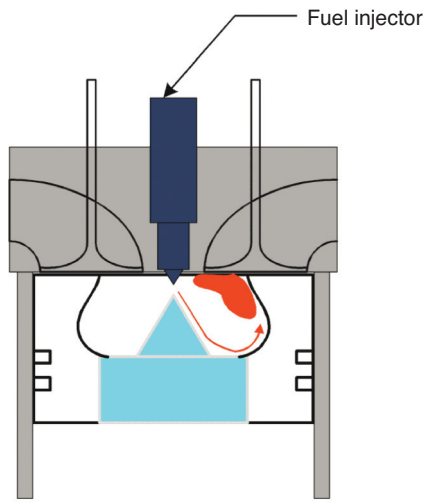

Figure 18

Schematic representation showing fuel trajectory and locally fuel-rich (stagnation zone) formed by piston bowl and cylinder head for late (near to TDC) SOI timings, wall-guided geometry.

The results presented within this section of the paper appear to reveal that the mechanism of bulk quenching is a major source of HC emissions in the wall-guided combustion chamber geometry. In the present study, quenching of the combustion zone is believed to occur as a result of two principal mechanisms. Firstly, bulk quenching can occur due to a temperature deficit. Results obtained on the all-metal engine have shown that the peak cycle temperature is a first order parameter which influences the engine-out HC emissions levels. In particular, a clear increase in the levels of unburned HC was observed with a reduction in peak cycle temperature, suggesting that bulk quenching was the mechanism responsible for the formation of unburned HC and in this case was a direct result of the low combustion temperatures. In-cylinder LIF imaging studies on the optical-access engine also revealed a noticeable increase in the level of in-cylinder unburned HC with a reduction of the intake temperature. This latter parameter was varied since it impacts the peak cycle temperature as shown in the present study.

Bulk quenching is also believed to occur as a result of undermixing of the fuel for late (near to TDC) SOI timings. In this case, the formation of a locally fuel-rich zone due to poor fuel-air mixing could lead to quenching of the HC oxidation reactions. The quenched combustion zone is susceptible to leave a layer or volume of unburned mixture. Although the subsequent oxidation of any remaining unburned HC might occur, it is less likely in the case of HCCI-type combustion since the in-cylinder temperatures attained are relatively low.

2.4 Liquid Film Formation

The wall-guided (NADI) combustion chamber system relies heavily on significant spray-wall interaction and in particular transport of the fuel mixture via the bowl-dome towards the re-entrant walls. However, the extent of spray-wall interaction and its effect on mixture distribution is clearly dependent on the SOI timing for a given nozzle and piston bowl geometry. For example, the fuel impingement location for advanced SOI timings in the range 280 to 330 CAD would inevitably differ in comparison with SOI timings nearer to TDC. In the present study, tracer LIF visualisations were performed with the objective of gaining an insight into the location of spray-wall impingement as a function of SOI timing. In particular, the potential of liquid fuel film formation and its importance as a source of HC emissions was studied. Within the present investigation, tracer LIF imaging was performed on the optical-access engine for the NADI combustion chamber geometry with variations of the SOI timing, engine coolant temperature and intake temperature whilst a "multi-fuel" approach was exploited on the all-metal engine. As explained earlier in the paper, the so-called "multi-fuel" approach adopted on the all-metal engine involved performing two series of experiments using two fuels of different volatilities.

2.4.1 All-Metal Engine Results – Effect of SOI Timing

The effect of SOI timing on HC emissions is shown in Figure 19 below for the all-metal engine. A comparison is made between the standard Diesel fuel and the higher volatility Fischer Tropsch (FT)/Kerosene blend. As explained earlier in the paper, the objective here was to perform tests using a higher volatility fuel which would allow us to isolate the role of liquid fuel films as a potential source of HC emissions without introducing adverse effects on the fuel distribution. In order to evaluate the validity of this assumption, experiments using the two fuels were performed on the all-metal engine using a conventional Diesel combustion chamber geometry (details provided earlier in the paper). In such combustion chamber geometries, the distance between the injector nozzle and piston bowl wall is greater compared to the wall-guided geometry which would be expected to limit the formation of liquid films. The results presented in Figure 19 for various SOI timings in the range 330 to 353 CAD obtained on the all-metal engine reveal very similar trends in terms of the HC emissions for both fuels. These results tend to confirm that the use of the higher volatility fuel blend has no significant effect on the HC emissions characteristics in a conventional Diesel combustion chamber geometry. One could therefore hypothesise that the use of the higher volatility kerosene fuel blend has no significant effect on the foregoing mixture preparation and combustion process (since it has been shown here that the HC emissions levels are influenced by factors such as the combustion phasing, maximum cycle temperature...). In summary, the results presented in Figure 19 give some credence to the "multi-fuel" approach used in this study as a means of investigating the phenomenon of liquid fuel films. Subsequent experiments were then performed on the wall-guided piston geometry.

HC emissions data obtained on the all-metal engine equipped with a wall-guided piston geometry are shown in Figure 20 for a wide range of SOI timings. Several notable features can be observed. Firstly, for SOI timings in the range 330 to 350 CAD, Figure 20 reveals very similar HC emissions levels for the two fuels. It should be noted that for this range of SOI timings, liquid film formation is expected to be minimal since significant spray-wall interaction occurs which results in a guiding effect of the fuel-air mixture, thus enhancing mixture preparation. In contrast however, for SOI timings in the range 300 to 330 CAD, one observes noticeable discrepancies in terms of the engine-out HC emissions. In particular, for the higher volatility FT/Kerosene fuel blend, the HC emissions are systematically lower compared to the standard Diesel fuel. Interestingly, it is in this range of SOI timings that the likelihood of fuel film formation is believed to occur since the fuel jets no longer interact with the bowl-dome but tend to impinge directly within the base of the piston bowl as shown schematically in Figure 21. Indeed, if liquid fuel film formation was believed to provide a possible mechanism for HC emissions then the use of a higher volatility fuel blend would be expected to minimise these effects since fuel film evaporation would be enhanced.

The results obtained on the all-metal engine and presented in Figure 20 tend to indicate that liquid fuel formation is likely

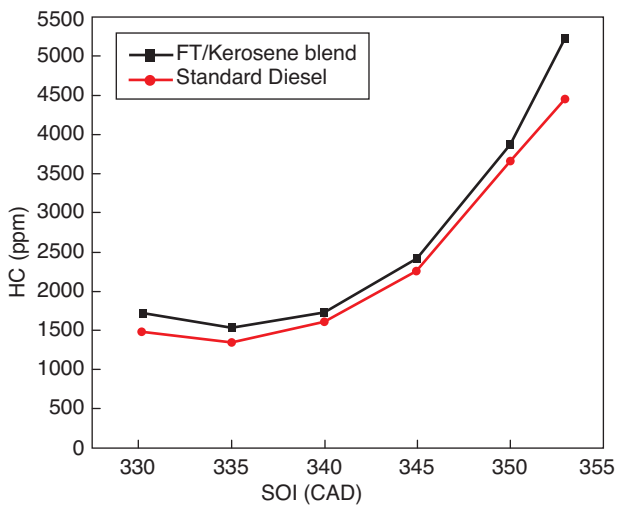

Figure 19

Comparison of HC emissions levels as a function of SOI timing for standard Diesel fuel and Fischer Tropsch/Kerosene blend, IMEP 2 bar, 45%EGR, 1500 rpm, all-metal engine data, conventional combustion chamber geometry.

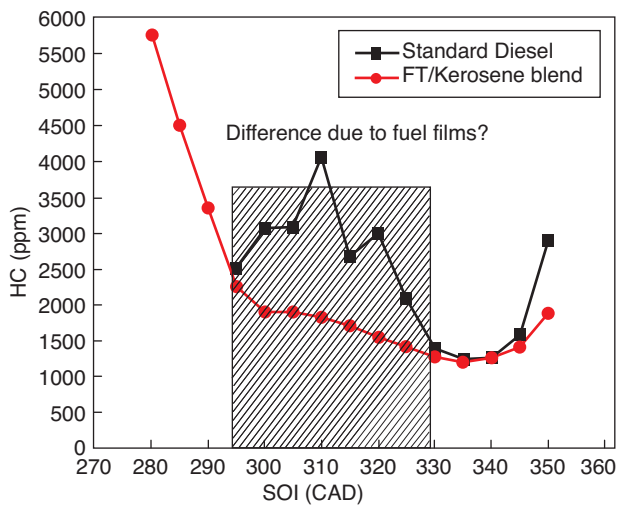

Figure 20

Comparison of HC emissions levels as a function of SOI timing for standard Diesel fuel and Fischer Tropsch/Kerosene blend, IMEP 2 bar, 45%EGR, 1500 rpm, all-metal engine data, wall-guided combustion chamber geometry.

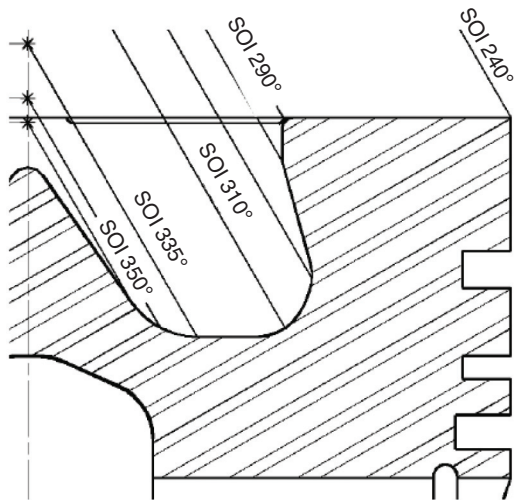

Figure 21

Schematic of the wall-guided geometry showing theoretical fuel jet trajectories and wall impingement locations for the nozzle and piston bowl geometry used in the present investigation for various SOI timings.

to occur in the case of the wall-guided geometry under certain SOI timing conditions and might explain the differences observed in the measured engine-out HC emissions. In order to study in greater detail the potential role of liquid films as a possible source of HC emissions in the wall-guided piston geometry, in-cylinder visualisations were performed on the optical-access engine using a tracer LIF technique to detect the presence of liquid films during and after combustion. For these experiments, particular focus was given to SOI timings in the range 310 to 320 CAD which are believed to be associated with the formation of fuel films.

2.4.2 Optical Engine Results - Effect of Intake Temperature

Figure 22 shows tracer LIF image sequences of the fuel as a function of the intake temperature ranging from 30 to 60°C for a SOI timing of 320 CAD (*i.e.* 40 CAD before TDC). This SOI timing was specifically selected since the fuel jets tend to impinge directly within the base of the piston bowl as shown by the schematic of Figure 21. Such SOI timing conditions would be thus considered favourable for the formation of liquid films since the fuel guiding effect would not intervene.

The LIF images presented in Figure 22 reveal the temporal and spatial evolution of the fuel mixture within the piston bowl.

The images show that the six fuel jets initially impact the base of the piston between the bowl dome and the re-entrant wall at approximately 325 CAD. For this particular

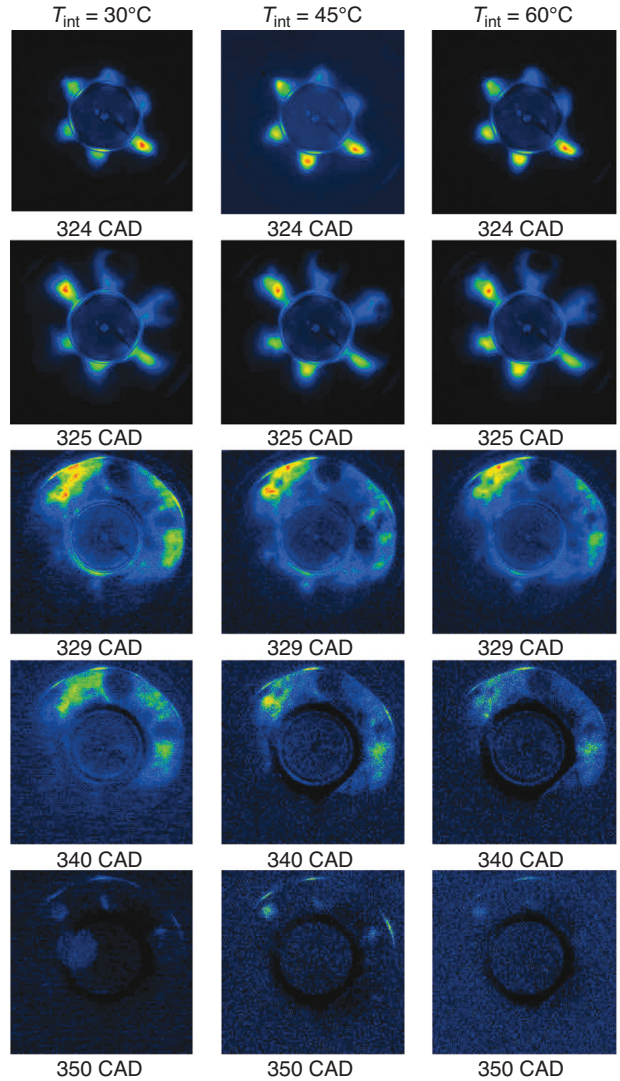

Figure 22

Image sequences of ensemble-averaged fuel tracer LIF images for various intake temperatures, EGR = 45%, 1200 rpm, SOI = 320 CAD.

SOI timing, the absence of significant wall-guiding effects on the subsequent jet trajectories may be expected to lead to the formation of fuel films. However it is not clear from the LIF images in Figure 22 whether the detected LIF signal corresponds to liquid or vapour phase fuel. At 329 CAD, the high LIF signal intensities reveal the presence of locally fuel-rich or stratified zones which are formed in distinct areas of the piston bowl. The spatial distribution of the LIF signal shows that the fuel is relatively dispersed within the piston bowl, indicating that the signal probably corresponds to fuel vapour. At approximately 340 CAD, the low LIF signal-to-noise ratio and the dispersed nature of the detected signal

seems to provide a further indication that the images obtained reveal the presence of fuel vapour. The LIF signal levels subsequently decrease to negligible levels and there is no indication, under these operating conditions of the presence of liquid fuel films.

In-cylinder pressure data which was acquired simultaneously with the LIF images reveals that the disappearance of the tracer LIF signal corresponds temporally with the start of the cool flame reactions, as indicated by the initial rise in the pressure trace at approximately 340 CAD *(Fig. 23)*. Although the combustion temperatures attained during the so-called cool flame stage are relatively low (up to approximately 700 K), they appear to be sufficient to ensure complete consumption of the remaining fuel vapour which remains within the piston bowl.

Surprisingly, the LIF images presented above revealed the apparent absence of fuel films, showing that the fuel (probably in vapour phase) was completely consumed during the early stages of the cool flame. It was hoped that this data would help to corroborate the trends observed on the all-metal engine in terms of the engine-out HC emissions data obtained using the "multi-fuel" approach. As a result it was not possible to confirm the possible link between the presence of liquid films and engine-out HC emissions. The results initially appeared contradictory since the all-metal engine data appears to indicate that fuel films do have a significant effect on HC emissions whilst the optical-access engine results show that the liquid films do not survive the combustion process. Possible reasons which might explain the somewhat contradictory results obtained from the two engines were considered. Particular consideration was given to the effect of wall temperature since experiments on the optical-access engine performed at a fully warmed-up engine condition (*i.e.* coolant temperature of 85°C) revealed the disappearance of fuel films at the start of combustion. However it should be noted that the actual wall temperature would be expected to be significantly higher on the optical access engine compared to the all-metal engine since the thermal conductivity of the quartz window used for optical access is an order of magnitude lower (K_{quartz} = 1.5 $Wm^{-1}K^{-1}$) compared to the aluminium-silicon alloy which is used for the fabrication of standard pistons ($K_{aluminium}$ = 121 $Wm^{-1}K^{-1}$). The lower thermal conductivity of quartz would inevitably lead to lower heat dissipation rates and would thus be expected to result in significantly higher wall temperatures. Furthermore, the combustion chamber of the all-metal engine is cooled via an underside oil-jet which directs oil (maintained at a temperature of 90°C) into an internal gallery machined into the piston head when the piston is at TDC. In contrast, the piston head of the optical-access engine is not cooled, providing yet more favourable conditions in which surface temperatures would be expected to reach higher values.

Higher wall surface temperatures would have a number of effects. Firstly, the expected differences in wall temperatures between the optical and all-metal engines would explain the discrepancies observed in terms of the combustion phasing shown earlier in the paper. It was shown that in the case of the optical-access engine, auto ignition was systematically advanced and this is believed to be due to different heat transfer effects between the walls and the bulk gases in the optical engine. This is an important result since it tends to confirm that wall to bulk gas heat transfer significantly influences the combustion phasing and pressure-rise rate (a more detailed analysis will be reported in a future paper). Secondly, the increased wall surface temperature would be expected to enhance fuel film evaporation. This might therefore explain why the LIF images obtained on the optical engine revealed an absence of fuel films during or after combustion for the warmed up engine condition (*i.e.* coolant temperature of 85°C) whilst in contrast, it would be possible in the case of the all-metal engine, that fuel films survive into the expansion and exhaust stroke due to the lower piston surface temperatures. In order to verify this, it would be necessary to perform LIF measurements whilst ensuring that the surface temperatures are maintained at comparable levels between the two engines. In order to simulate more closely the conditions encountered in the all-metal engine with regards to the wall temperature, in-cylinder LIF imaging was performed at various engine coolant temperatures. Results are presented in the following sub-section. Clearly a quantitative measure of piston temperature would be required in order to replicate precisely the conditions encountered in the all-metal engine and such a technique is currently being

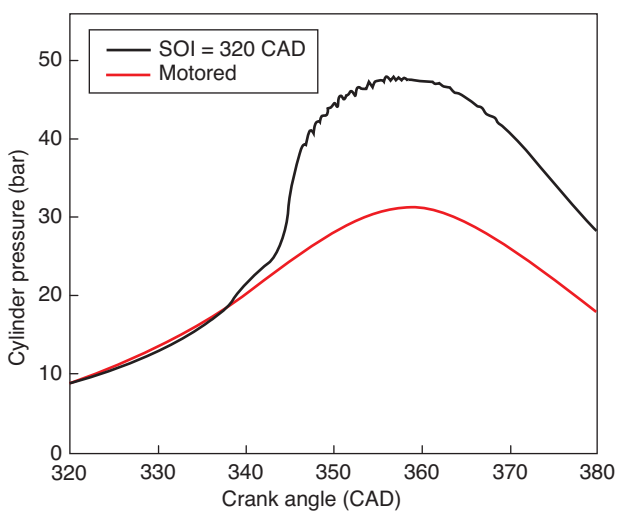

Figure 23

In-cylinder pressure trace for SOI = 320 CAD showing start of cool flame at ~340 CAD, EGR = 45%, T_{int} = 60°C.

developed at IFP. Finally, it should also be reminded that for the tracer-LIF imaging experiments, dodecane fuel was used which has a much higher volatility compared to standard Diesel fuel *(Table 2)*. As a result, fuel evaporation rates would be higher which would tend to reduce the likelihood of fuel film formation.

2.4.3 Optical Engine Results - Effect of Coolant Temperature

As explained above, a combination of several factors such as the lower thermal conductivity of quartz, an absence of an oil jet for piston head cooling and the higher fuel volatility of dodecane fuel characteristics are all expected to reduce the likelihood of fuel film formation on the optical-access engine. This brings into question the reliability of the optical engine in terms of being able to reproduce the conditions occurring in the all-metal engine for the study of fuel film formation since wall surface temperature would have a significant influence on this phenomenon. In order to simulate more accurately the wall temperature conditions which would likely be encountered on the all-metal engine, the coolant temperature was decreased. LIF imaging of the fuel distribution was performed for a variation of coolant temperature at a fixed SOI timing of 320 CAD. Figure 24 shows ensemble-averaged images for coolant temperatures of 40, 60 and 85°C. A short time after the end of injection, at 330 CAD, the images show that a moderate decrease of the coolant temperature from 85 to 60°C appears to have relatively little influence on the fuel spatial distribution. One observes two distinct zones of locally elevated fuel concentration (most likely corresponding to fuel vapour taking into account the dispersed spatial distribution) at the 11 o' clock and 4 o' clock positions within the piston bowl. In contrast however, a further decrease of the coolant temperature from 60 to 40°C reveals a significant effect. At 330 CAD, one clearly observes six distinct zones which are formed following impingement of the fuel jets from the six-hole nozzle. The difference in spatial distribution of the detected LIF signal induced by a decrease in the coolant temperature tends to indicate a lower degree of fuel dispersion and evaporation. The zones observed are therefore believed to correspond to liquid fuel. At 340 CAD, corresponding to the early stages of the cool flame (the combustion phasing is retarded with a progressive decrease in the coolant temperature as shown by the acquired in-cylinder pressure data: *Fig. 25*), the detected LIF signal levels decrease to very low levels at the coolant temperature of 85°C. As observed earlier, the LIF signal, probably corresponding to vapour phase fuel disappears shortly after 340 CAD, revealing a complete absence (or at least undetectable levels) of fuel within the piston bowl. At the intermediate coolant temperature of 60°C, the LIF images appear to show that liquid fuel films survive later into the cycle and are clearly observed at TDC, by which time the high temperature combustion is already well underway. This trend is further amplified at the lowest coolant temperature of 40°C. In this latter case, the LIF images reveal distinct zones of high intensity and it is now clear that these zones correspond to liquid fuel films on the piston surface since the spatial location of the fuel remains unchanged throughout the cycle, from just after the end of injection at 330 CAD until late into the expansion stroke at 400 CAD. Furthermore, any remaining fuel vapour, present within the bulk gases would have otherwise been consumed during combustion. Although the LIF data presented here is purely qualitative (no attempt has been made to quantify the fuel mass or film thickness), higher LIF signal intensities are detected with a decrease in coolant temperature, indicating higher fuel concentrations. The optical filter set used in these experiments enabled unambiguous detection of the presence of fuel films. Furthermore, the LIF images presented in Figure 24 confirm that fuel film visualisation was possible under reacting conditions (*i.e.* signal interference due to high intensity combustion luminosity did not pose major problems).

The results presented in Figure 24 reveal the significant effect of coolant temperature on the formation of liquid fuel films. Decreasing the coolant temperature leads to a decrease of the combustion chamber wall temperature which would be expected to simulate more realistically the conditions encountered in the all-metal engine. Indeed the LIF imaging data obtained at a reduced coolant temperature revealed the presence of liquid fuel films well after the end of combustion which corroborates the explanation given earlier that liquid films may be responsible for the increased HC emissions for early SOI timings (as revealed using the "multi-fuel" engine data). These findings have quite significant implications since one would therefore expect the role of fuel films to be more preponderant in the all-metal engine due not only to a combination of lower piston surface temperatures but also the presence of high boiling point compounds within standard Diesel fuel. Finally, the optical engine results obtained at the coolant temperature of 85°C *(Fig. 24)* which revealed an absence of fuel films also correlate well with the HC emissions trends shown in Figure 8. One observed in Figure 8 that the engine-out HC emissions levels were noticeably lower using dodecane fuel compared to standard Diesel fuel for the range of SOI timings (SOI between 300 and 330 CAD) which are believed to favour the formation of fuel films. Indeed, the results shown in Figure 8 did not reveal an increase in the HC emissions in this range of SOI timings for the high volatility dodecane fuel, contrary to the results obtained with standard Diesel fuel.

2.4.4 Optical Engine Results - Effect of Injection Timing

The results presented above revealed the significant effects of engine coolant temperature on the formation of piston-top fuel films. The above results were shown for a fixed injection timing (SOI at 320 CAD) which is known to result in significant fuel splashing/impingement within the base of the piston bowl. As a result, fuel recirculation and subsequent mixing

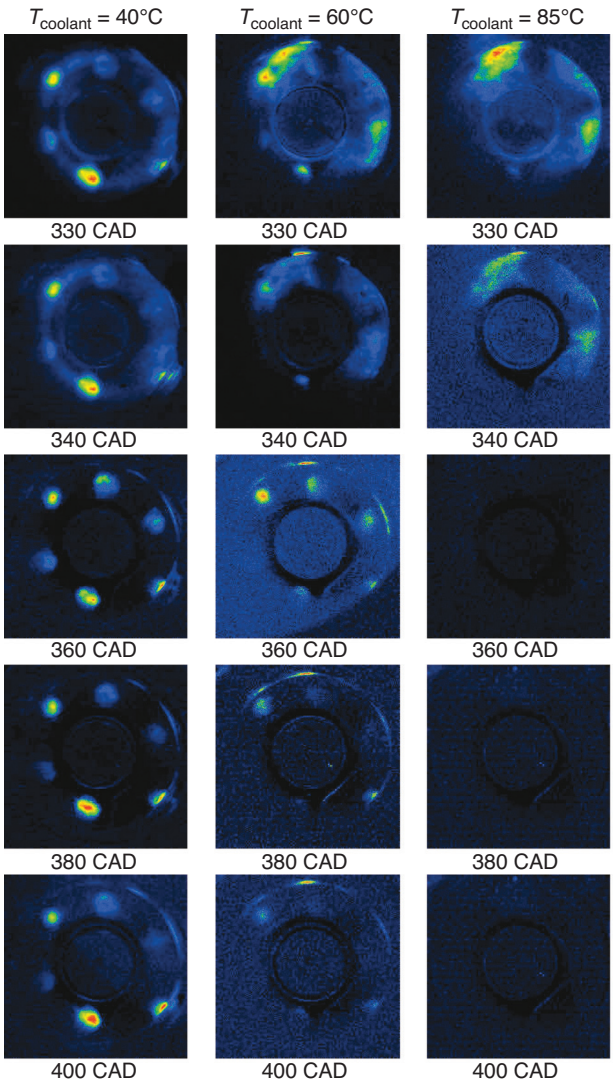

Figure 24

Image sequences of ensemble-averaged fuel tracer LIF images showing effect of engine coolant temperature on presence of fuel films, SOI = 320 CAD, EGR = 45%, 1200 rpm, T_{int} = 60°C. Note: Colour mapping optimised for each image.

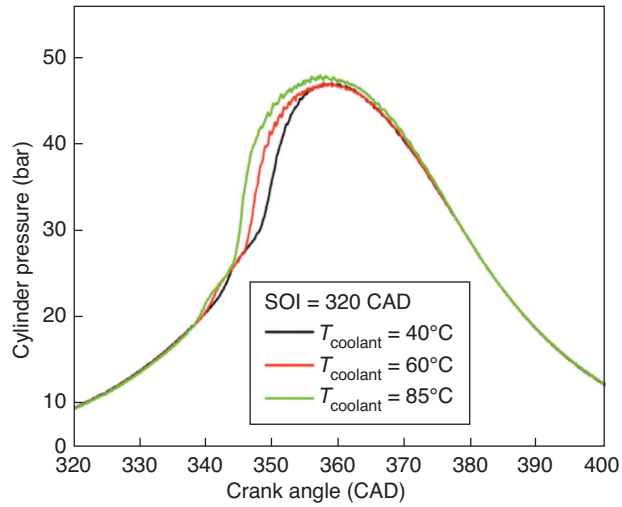

Figure 25

In-cylinder pressure traces for varying engine coolant temperatures at fixed SOI = 320 CAD, EGR = 45%, T_{int} = 60°C.

with the surrounding air within the combustion chamber is very limited. Tracer LIF imaging was subsequently performed in order to determine whether fuel film formation was as prevalent for other injection timings whilst maintaining an engine coolant temperature of 40°C. Three sequences of ensemble-averaged tracer LIF images are shown in Figure 26 corresponding to SOI timings of 300, 320 and 340 CAD.

For a SOI timing at 300 CAD, the images reveal the presence of six distinct zones (at 306 CAD) corresponding to the locations of fuel impingement. The images at 309 and 335 CAD reveal a more dispersed LIF signal. For this SOI timing, combustion begins at approximately 345 CAD, however the LIF image obtained at 415 CAD, well after the end of combustion, confirms the presence of liquid films around the periphery of the bowl wall. Data obtained for the SOI timing at 320 CAD is presented again in Figure 26 so as to enable a direct comparison. As discussed earlier in the paper, this SOI timing leads to significant fuel splashing in the base of the piston bowl and subsequently very limited recirculation of the fuel mixture. As a result, fuel films are detected throughout the cycle and late into the expansion stroke. In contrast, the SOI timing at 340 CAD reveals a different sequence of events. The fuel jets are believed to impinge at the base of the bowl-dome leading to significant radial and axial dispersion of the fuel. Indeed, the spatial distribution of the LIF image obtained at 345 CAD clearly shows significant radial spreading of the fuel and a distinct absence of fuel accumulation within the base of the piston bowl. Contrary to the early SOI timings (300 and 320 CAD) mixture preparation is enhanced due to the fact that the fuel jets are guided towards the re-entrant. These data thus confirm that the SOI timing has a considerable effect on the formation of liquid films. Furthermore, the LIF data corroborates the HC emissions trends observed on the all-metal engine *(Fig. 20)*. A comparison of the HC emissions data obtained on the all-metal engine for standard Diesel fuel and the higher volatility fuel revealed noticeable differences for SOI timings in the range 300 to 330 CAD. The LIF data presented here has indeed confirmed that these injection timings result in the formation of liquid films. On the contrary, all-metal engine data revealed similar HC emissions levels for both fuels for SOI timings which appear to result in minimal fuel film formation (*i.e.* SOI timings in the range 335 to 350 CAD).

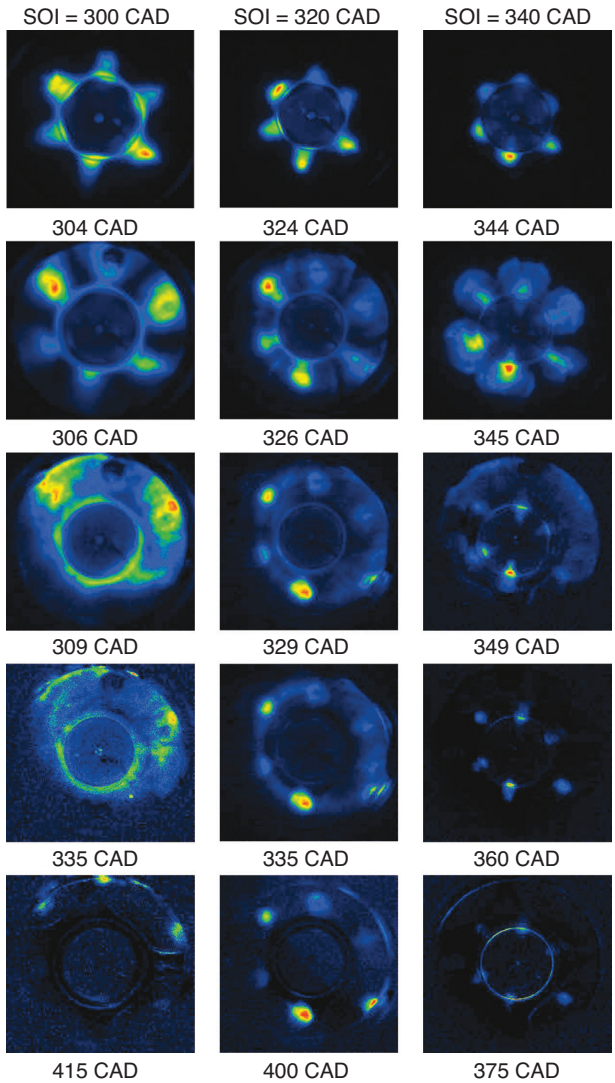

Figure 26

Image sequences of ensemble-averaged fuel tracer LIF images showing effect of SOI timing liquid fuel film formation for $T_{coolant}$ = 40°C, EGR = 45%, 1200 rpm, T_{int} = 60°C. Note: Colour mapping optimised for each image.

LIF imaging experiments were performed with particular focus given to the presence of fuel films late in the engine cycle.

Figure 27 shows three ensemble-averaged tracer LIF images of the fuel film acquired late in the expansion stroke and early in the exhaust stroke (from 500 CAD). The image acquired at 480 CAD reveals the presence of liquid fuel films at distinct, equally spaced zones around the piston bowl corresponding to the locations of jet impingement. At 500 CAD upon exhaust valve opening, the liquid films are still detectable although the LIF image signal-to-noise level is clearly reduced. Later on into the exhaust stroke, one observes a distinct change in the spatial distribution of the LIF signal corresponding to the fuel film. At 540 CAD, the LIF signal is no longer confined to distinct zones on the piston surface but appears rather dispersed, resembling a cloud of fuel droplets and/or fuel vapour. The acquired LIF images revealed that this characteristic was repeatable from cycle-to-cycle. A plausible explanation as to the process occurring in-cylinder is that the fuel films, either partially or completely detach from the piston surface. This could be due to fuel film flash boiling, a mechanism whereby the liquid phase fuel is suddenly vaporised as a result of a rapid pressure decrease to below the fuel vapour pressure. The fuel which is deposited on the piston surface is in the liquid phase and it can be assumed that the film thickness is sufficiently small that its temperature is comparable to the wall temperature. As a result of the decrease of in-cylinder pressure during the expansion and exhaust strokes, it is possible that the liquid film detaches from the piston surface, forming a cloud of fuel droplets. It is possible that fuel flash boiling might induce a phase change from liquid to vapour.

The pressure-temperature diagram of Figure 28 shows schematically the phase change from liquid to vapour (then potentially back to liquid) that might be occurring in-cylinder as a result of flash boiling.

The liquid film (A) present on the piston surface would be expected to have a temperature close to the wall surface temperature and would undergo a rapid decrease in pressure and

2.4.5 Consequences of Liquid Fuel Film Formation on Combustion and HC Emissions

The tracer LIF imaging data revealed the presence of liquid fuel films late into the expansion stroke and the influence of wall temperature on the formation and lifetime of these fuel films. The question then arises as to the fate of the liquid films on exhaust valve opening and in particular, whether a correlation between the presence of fuel films and the measured engine-out HC emissions can be established. In an attempt to respond to these questions, further

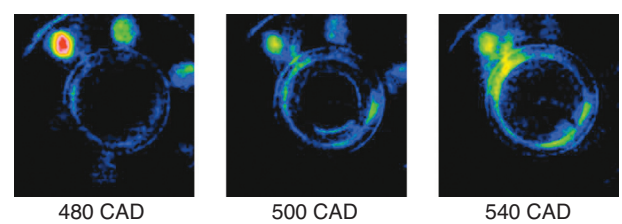

Figure 27

Ensemble-averaged tracer LIF images showing break-up of liquid fuel films via flash boiling, $T_{coolant}$ = 40°C, EGR = 45%, T_{int} = 60°C, SOI = 320 CAD.

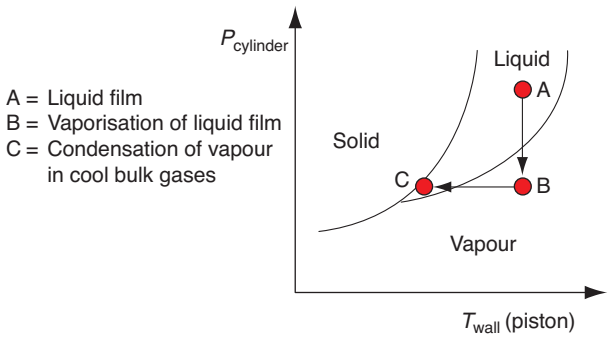

Figure 28

2D pressure-temperature diagram for the dodecane-5-nonanone fuel-tracer mixture showing possible phase transitions occurring during film flash boiling.

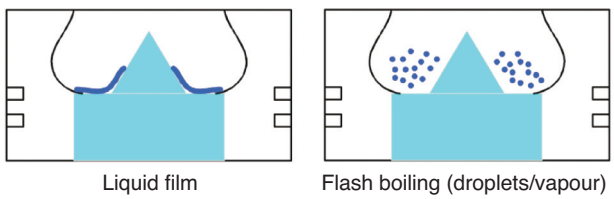

Figure 29

Schematic showing mechanism of flash boiling of liquid film during expansion/exhaust stroke and emission of unburned HC.

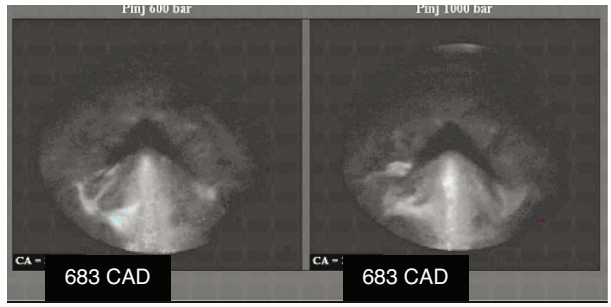

Figure 30

In-cylinder images obtained by endoscope in the all-metal engine reveals the presence of a fuel cloud during the exhaust stroke, 1500 rpm, 2 bar IMEP, SOI = 340 CAD.

temperature during the expansion stroke (B). At these new in-cylinder pressure and temperature conditions, it is believed that the fuel film subsequently detaches from the piston surface, resembling a flash boiling phenomenon and might induce a phase change from liquid to vapour. A fuel cloud is then formed above the piston surface consisting of fuel droplets and vapour (C) which is subsequently emitted into the exhaust gases. The mechanism of film flash boiling occurring late during the expansion or exhaust stroke is therefore believed to contribute directly to the measured engine-out HC emissions. Indeed fuel film formation is believed to occur for relatively early SOI timings between 300 and 330 CAD and it is indeed for these SOI timings that elevated levels of unburned HC emissions are observed.

The schematic of Figure 29 shows the flash boiling phenomenon whereby liquid fuel deposited on the piston top surface in the form of a film rapidly boils, producing a cloud of fuel droplets and/or vapour. Subsequently, this fuel cloud would presumably be emitted with the remaining burned gases on exhaust valve opening. Although some degree of post-oxidation may occur, this is less likely given the low exhaust gas temperatures at such low load operating conditions and it is thus possible that the emitted unburned HC contributes directly to the measured engine-out HC emissions.

The LIF images obtained late in the exhaust stroke which appear to show the fuel film detaching from the piston surface seem to corroborate in-cylinder visualisations performed by endoscopy in the all-metal engine. The images obtained by endoscopy were performed for a similar engine operating condition (*i.e.* 1500 rpm, 2 bar IMEP) and for a range of SOI timings. Images acquired late into the expansion and early during the exhaust stroke revealed the presence of a cloud-like structure believed to be due to Mie scattering (elastically-scattered light) of fuel droplets which have detached from the piston surface. Two typical images acquired by endoscopy in the all-metal engine are shown in Figure 30 for two different injection pressures (600 and 1000 bar). The images are obtained very late into the exhaust stroke at 683 CAD (*i.e.* 323 CAD after TDC compression). The unburned fuel would then presumably be drawn out of the cylinder with the burned exhaust gases.

Although the primary focus of the present study was to investigate and attempt to identify potential HC formation mechanisms, imaging of natural combustion luminosity (chemiluminescence and soot incandescence) was performed in order to study the impact of fuel films on the subsequent combustion process. Direct imaging of the naturally emitted light was performed using a 16-bit intensified CCD camera (*Roper Scientific PIMAX*) and 105 mm objective lens (f/2.8). Combustion imaging data was acquired for the early SOI timing at 320 CAD and for two coolant temperatures of 40 and 85°C, corresponding to cold-start and warmed-up engine operating conditions respectively. Maximum camera gain was used whilst the gate (exposure) time was adjusted as necessary in order to optimise image signal-to-noise ratio. The gate times were typically varied in the range 30 to 80 μs.

Two sequences of ensemble-averaged (averaged over 50 consecutive engine cycles) images of the combustion process are shown in Figure 31 corresponding to the two coolant temperatures. It should be noted that the colour map scales have been optimised so as to highlight the information contained

within the images. At 350 CAD, one observes the initial, relatively weak chemiluminescence emission due to low temperature oxidation reactions, commonly referred to as the "cool-flame". In the early stages of combustion, at 350 CAD, the images obtained are very similar regardless of the coolant temperature. Near to TDC however, the images reveal significant differences in terms of the signal spatial distribution. Under warmed-up engine conditions at 85°C, the signal is relatively homogeneous throughout the combustion chamber whereas at the lower coolant temperature condition, localised zones of high signal intensity are observed. Furthermore, these zones correspond spatially to zones where liquid fuel films are known to exist. The high signal intensities that are detected are typical of sooting combustion and is believed to be due to pool-firing of the liquid films. Such phenomena have previously been observed in both gasoline direct injection and port-injection engines using optical diagnostics [18-20]. The high signal intensities of soot incandescence clearly dominates the chemiluminescence intensity of other emitting species that may be present. Under warmed-up engine conditions, the combustion images tend to reveal a homogeneous structure cycle until approximately 385 CAD, thereafter, the signal levels reduce to negligible levels. In contrast, at the lower coolant temperature of 40°C, localised pool fires are detected late into the expansion stroke, characterised by high signal intensities. The liquid fuel films burn as fuel-rich diffusion flames thus producing, locally at least, elevated levels of soot.

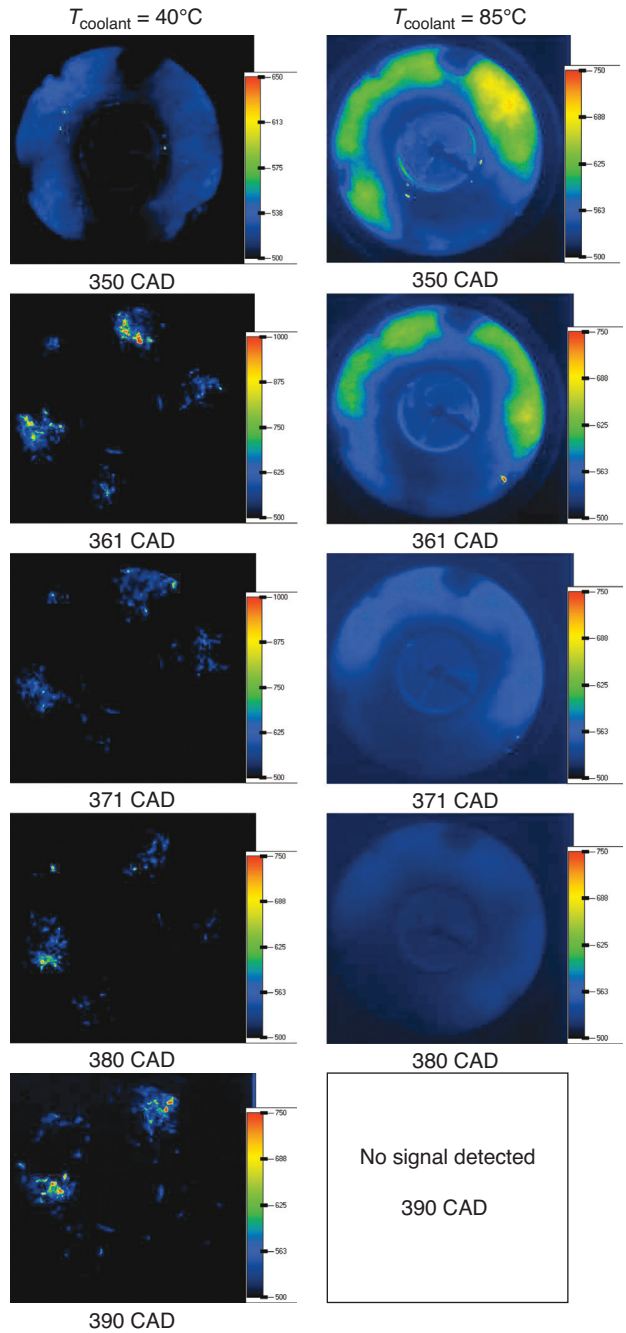

Figure 31

Ensemble-averaged chemiluminescence images showing effect of engine coolant temperature on combustion development, SOI = 320 CAD, EGR = 45%, 1200 rpm, T_{int} = 60°C. Note: Colour mapping optimised for each image.

SUMMARY AND CONCLUSIONS

The origin and mechanisms of unburned HC emissions in a wall-guided, low temperature Diesel combustion have been investigated on an all-metal and equivalent optical-access single cylinder engine. In order to assess the relative importance of several potential sources of HC emissions as a function of SOI timing, a variety of experimental methods were exploited. Firstly, the importance of the piston topland crevice volume as a potential source of HC emissions via fuel trapping was studied on the all-metal engine. Secondly, the role of bulk quenching was studied via in-cylinder LIF imaging of unburned HC on the optical engine whilst variations of equivalence ratio and intake temperature were performed on the all-metal engine. Finally, the phenomenon of liquid fuel film formation and its potential role on HC emissions was investigated on the all-metal engine using a "multi-fuel" method (*i.e.* two fuels of different volatilities) whereas in-cylinder tracer LIF imaging enabled complementary studies to be performed on the optical engine.

The results presented in this paper provide an insight into the sources of HC emissions formation for a wall-guided, low NOx, Diesel combustion system. In particular, the mechanisms of HC formation identified within this study have enabled us to clarify the reasons why the SOI timing has such a significant impact on the HC emissions. Figure 32 summarises the principal mechanisms which are believed to be responsible for early through late SOI timings.

The results presented in this paper have shown bulk quenching to be a major source of unburned HC emissions.

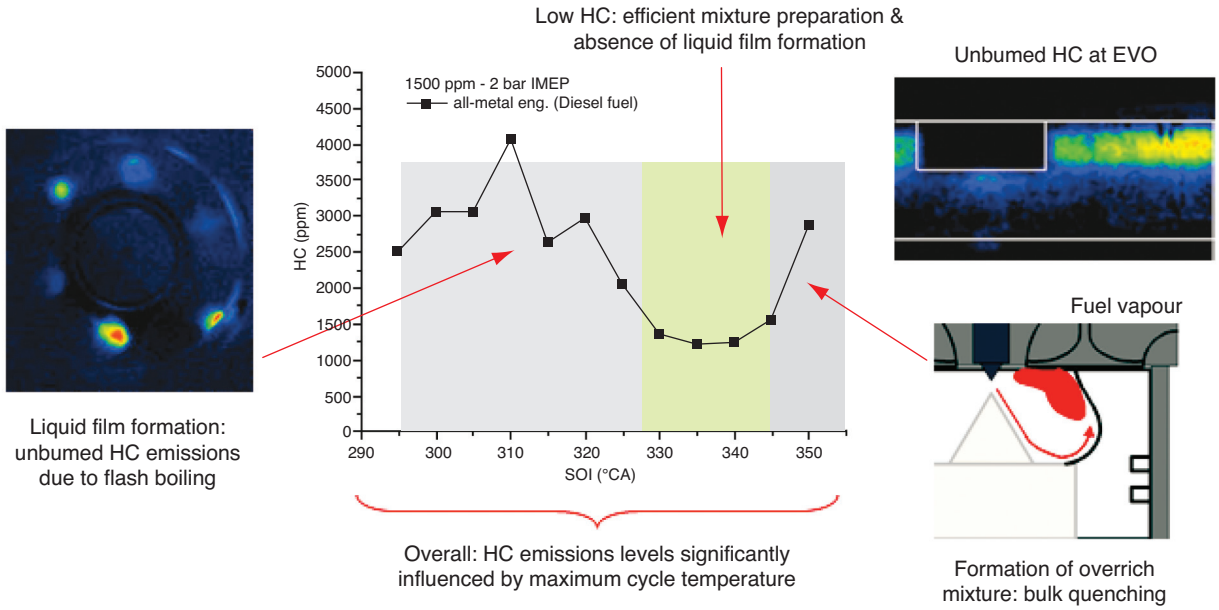

Figure 32

Summary of the potential mechanisms of HC formation identified in the present study as a function of SOI timing for a wall-guided, low NOx combustion system.

In particular, a clear correlation appears to exist between the maximum cycle temperature and the measured engine-out HC emissions. As a result, the presence of thermal inhomogeneities (*e.g.* the formation of low temperature zones) could potentially result in quenching of the combustion zone, thereby preventing the combustion reactions from going to completion. The bulk quenching mechanism is also believed to occur as a result of the local equivalence ratio distribution. In particular, the formation of locally over-rich zones due to under mixing of the fuel is believed to occur for late SOI timings near to TDC since the injected fuel is strongly convected via the bowl dome and re-entrant geometry. As a result, a locally fuel-rich mixture zone is formed due to confinement by the piston bowl lip and the cylinder head *(see Fig. 32)*. Quenching within the bulk gases is believed to take place in this zone due to insufficient oxygen available to fully oxidise all of the available fuel.

For early SOI timings in the range 300 to 330 CAD, the fuel jets are expected to impinge directly on the base of the piston bowl potentially leading to the formation of liquid fuel films. The fate of these fuel films throughout the combustion process and late into the expansion stroke was studied using a tracer LIF technique. At reduced engine coolant temperature, the results presented tended to confirm the presence of liquid fuel films late into the expansion stroke and at exhaust valve opening. Furthermore, it is believed that the fuel films which remain late in the cycle subsequently detach from the piston surface and are emitted into the exhaust gases. Indeed tracer LIF images showed that the spatial distribution of the signal rapidly changes, indicating perhaps a phase change (from liquid to vapour) or the formation of a cloud of droplets. It was proposed that flash boiling might occur due to the combined effects of the fuel film being heated by the hot piston wall and the rapid decrease of in-cylinder pressure during expansion. This mechanism would explain how fuel films might directly contribute to the level of engine-out HC emissions. Indeed, the optical engine results seem to corroborate the all-metal engine data regarding the role of liquid fuel films on HC emissions. In the latter case, HC emissions data obtained using standard Diesel and a higher volatility fuel revealed significantly differences in the range of SOI timings susceptible to the formation of liquid films. The lower level of HC emissions observed with the higher volatility fuel is believed to be directly linked to the preferential evaporation and oxidation of these fuel films prior to exhaust valve opening. Furthermore, in-cylinder images obtained via an endoscope on the all-metal engine appeared to confirm the presence of late cycle fuel films.

The role of the piston top land crevice volume as a potential source of HC emission was studied on the all-metal engine. However, increasing the top land crevice volume by a factor of two did not lead to any noticeable increase in the measured engine-out HC emissions over the range of SOI timings between 300 and 355 CAD. These findings confirmed

that the top land crevice volume has a negligible effect on the unburned HC emissions in the wall-guided combustion geometry used in the present study.

ACKNOWLEDGMENTS

This research was conducted within the framework of a research program funded by the Groupement Scientifique Moteurs (*IFP, PSA* and *Renault*) for which financial support is gratefully acknowledged.

REFERENCES

1 Christensen M., Johansson B., Hultqvist A. (2001) The Effect of Piston Topland Geometry on Emissions of Unburned Hydrocarbons from a Homogeneous Charge Compression Ignition (HCCI) Engine, *SAE technical paper* 2001-01-1893.

2 Aceves S.M., Flowers D.L., Espinoza-Loza F., Martinez-Frias J., Dibble R.W., Christensen M., Johansson B., Hessel R.P. (2002) Piston-Liner Crevice Geometry Effect on HCCI Combustion by Multi-Zone Analysis, *SAE technical paper* 2002-01-2869.

3 Heywood J.B. (1988) *Internal Combustion Engine Fundamentals*, McGraw-Hill, New York.

4 Iida M., Hayashi M., Foster D.E., Martin J.K. (2003) Characteristics of Homogeneous Charge Compression Ignition (HCCI) Engine Operation for Variations in Compression Ratio, Speed and Intake Temperature while using n-Butane as a Fuel, *Trans. ASME* **125**, 472-478.

5 Kook S., Bae C., Miles P.C., Choi D., Pickett L.M. (2005) The Influence of Charge Dilution and Injection Timing on Low-Temperature Diesel Combustion and Emissions, *SAE technical paper* 2005-01-3837.

6 Kook S., Bae C., Miles P.C., Choi D., Bergin M., Reitz R.D. (2006) The Effect of Swirl Ratio and Fuel Injection Parameters on CO Emission and Fuel Conversion Efficiency for High-Dilution, Low-Temperature Combustion in an Automotive Diesel Engine, *SAE technical paper* 2006-01-0197.

7 Kashdan J.T., Docquier N., Bruneaux G. (2004) Mixture Preparation and Combustion via LIEF and LIF of Combustion Radicals in a Direct-Injection, HCCI Diesel Engine, *SAE technical paper* 2004-01-2945.

8 Walter B., Gatellier B. (2002) Development of the High Power NADI Concept Using Dual Mode Diesel Combustion to Achieve Zero NOx and Particulate Emissions, *SAE technical paper* 2002-01-1744.

9 Siebers D.L. (1998) Liquid-Phase Fuel Penetration in Diesel Sprays, *SAE technical paper* 980809.

10 Siebers D.L. (1999) Scaling Liquid-Phase Fuel Penetration in Diesel Sprays Based on Mixing-Limited Vaporization, *SAE technical paper* 1999-01-0528.

11 Kimura S., Aoki O., Kitahara Y., Aiyoshizawa E. (2001) Ultra-Clean Combustion Technology Combining a Low-Temperature and Premixed Combustion Concept For Meeting Future Emissions Standards, *SAE technical paper* 2001-01-0200.

12 Lachaux T., Musculus M.P.B. (2006) In-Cylinder Unburned Hydrocarbon Visualisation During Low-Temperature Compression-Ignition Engine Combustion Using Formaldehyde PLIF, *Proc. 31st Combustion Symp. 2006*, Heidelberg, Germany, 6-11 August 2006.

13 Kashdan J.T., Papagni, J.-F. (2005) LIF Imaging of Auto-Ignition and Combustion in a Direct-Injection Diesel-Fuelled, HCCI Engine, *SAE technical paper* 2005-01-3739.

14 Schulz C., Gronki J., Andersson S. (2004) Multi-Species Laser-Based Imaging Measurements in a Diesel Spray, *SAE technical paper* 2004-01-1917.

15 Bruneaux G. (2007) Study of the Correlation Between Mixing and Auto-ignition Processes in High Pressure Diesel Jets, *SAE technical paper* 2007-01-0650.

16 Sjöberg M., Dec J.E., Babjimopoulos A., Assanis D. (2004) Comparing Enhanced Natural Thermal Stratification against Retarded Combustion Phasing for Smoothing of HCCI Heat-Release Rates, *SAE technical paper* 2004-01-2994.

17 Dec J.E., Hwang W., Sjöberg M. (2006) An Investigation of Thermal Stratification in HCCI Engines using Chemiluminescence Imaging, *SAE technical paper* 2006-01-1518.

18 Stevens E., Steeper R. (2001) Piston Wetting in an Optical DISI Engine: Fuel Films, Pool Fires and Soot Generation, *SAE technical paper* 2001-01-1203.

19 Witze P.O., Green R.M. (1997) LIF and Flame-Emission Imaging of Liquid Fuel Films and Pool Fires in an SI Engine During a Simulated Cold Start, *SAE technical paper* 970866.

20 Witze P.O., Green R.M. (2005) Comparison of Single and Dual Spray Fuel Injectors During Cold Start of a PFI Spark-Ignition Engine Using Visualization of Liquid Fuel Films and Pool Fires, *SAE technical paper* 2005-01-3863.

21 Dec J.E. (2002) A Computational Study of the Effects of Low Fuel Loading and EGR on Heat Release Rates and Combustion Limits in HCCI Engines, *SAE technical paper* 2002-01-1309.

22 Dec J.E., Sjöberg M. (2003) A Parametric Study of HCCI Combustion – The Sources of Emissions at Low Loads and the Effects of GDI Fuel Injection, *SAE technical paper* 2003-01-0752.

23 Marriott C.D., Reitz R.D. (2002) Experimental Investigation of Direct Injection Gasoline for Premixed Compression Ignited Combustion Phasing Control, *SAE technical paper* 2002-01-0418.

Final manuscript received in September 2007
Published online in July 2008